LABORATORY MODELS OF MICROBIAL BIOSIGNATURES IN CARBONATE

ROCKS

Thesis by

Tanja Bosak

In Partial Fulfillment of the Requirements

for the Degree of

Doctor of Philosophy

California Institute of Technology

Pasadena, California

2005

(Defended December 8, 2004)

ACKNOWLEDGMENTS

When I tell people that I'm a geomicrobiologist, there's usually a blank stare and an "Uh-huh" that follows. Then, when I say that it is all about early life on Earth and how to tell whether microbes made some really, really old rocks, the eyes light up and the ears perk up, wanting to learn more about both microbes and rocks. What I usually don't have the chance to tell people is that they can hear all these stories from me because of one person, my advisor, Dianne Newman. We met when her lab here at Caltech was in a very early developmental stage, and my microbiological self in an even earlier. She bravely took me on, watched without a word when I almost set her lab on fire, encouraged me and taught me how to be rigorous and the meaning of "the". Throughout these four years, Dianne has been equally excited about the smallest experiments and about larger stories that they described. Without her optimism and support, all these stories about microbes and rocks might have never left all those test tubes.

Microbes, rocks and Dianne's positive attitude, not surprisingly, proved irresistible to the people that have passed through the Newman lab for the past five years. I cannot imagine sharing a lab, food, and scientific experience with a better group of people and want to thank all of you for being yourselves and being there. Outside the lab, Joe Kirshvink has been an endless source of creative ideas and great field trips. As my advisor during a very rough first year at Caltech, Andy Ingersoll showed great understanding and I'll always be inspired by his ability to ask the right questions to get to the core of a problem. Ben Weiss has provided a very Martian perspective on both life and science and has kept me grounded, although we are still unsure on which planet. In

Appendix 1. Shannon Greene, a Caltech sophomore, learned about stromatolites by growing and counting phototrophic bacteria, taking ICP-MS samples, and taught the Newman lab a thing or two about Texas, country music, and Vegas. A lot of the observations and measurements in this part would not have happened without Shannon's excitement and dedication. The Agouron Institute (Bosak), Luce, and Packard Foundations (Newman) provided financial support.

Last, but not the least, my friends and fellow students in GPS and in the L.A. area, Elisabeth, the Smith-Downeys, David, Helene, Mo, Ed, Chris, Juancarlos, Jen, Sara and many others have provided much needed conversations, parties, pumpkin cakes, dinners, trips to the desert, the beach, and the local Peet's. These five-and-some years would have been much different without you.

ABSTRACT

Enigmatically shaped laminated carbonate rocks called stromatolites dominated shallow marine environments for the first 80% of Earth's history, and are potentially the oldest macrofossils. While these ancient rocky cones and domes occasionally resemble some modern microbial structures, it is unclear whether their formation required biological processes or they could have been produced abiotically. To develop criteria for assessing the biogenicity of ancient stromatolites, we precipitated calcium carbonate in the laboratory in the presence and absence of modern microorganisms under chemical conditions relevant for the early Earth. Using this novel approach, we disproved the paradigm that microbial sulfate reduction, a metabolism important for the formation of modern stromatolites, was responsible for the precipitation of their ancient counterparts. We also produced the first laboratory evidence that sub-micron and micron-sized pores occured in rapidly precipitating carbonate rocks only when microbes were present. Applying a set of experimentally established criteria to modern environmental samples and ancient stromatolites, we found similar biogenic microporosity in some modern fast-precipitating carbonates and in ancient stromatolites. In our abiotic laboratory precipitates, we observed calcite grains that resembled putatively biogenic features from the rock record called peloids. We explained their shape and growth pattern by purely inorganic parameters, underscoring the need for caution when interpreting seemingly biogenic fabrics in the rock record of Earth and other planets. Finally, we showed that active anoxygenic photosynthesis by *Rhodopseudomonas palustris* could stimulate the precipitation of calcite even in solutions that were well-buffered by a high concentration

of dissolved inorganic carbon. Future studies of the relationship between photosynthetic biofilms, the environmental parameters such as light and currents, and the morphology of carbonate precipitates are key to recognizing potential biosignatures produced by similar organisms in the *in situ* precipitated stromatolites and other microbialites.

TABLE OF CONTENTS

LIST OF FIGURES

LIST OF TABLES

1. Introduction

Are stromatolites the oldest macrofossils?

Stromatolites are laminated and lithified carbonate rocks that dominated shallow marine environments for the first 80% of Earth's history. Because the centimeter and decimeter-sized domical and conical shapes of ancient stromatolites are similar to some rare modern-day microbially-dominated structures, such as those found in Shark's Bay, Australia and the Bahamas, the term stromatolite is used to refer to both. Even the oldest stromatolites (~ 3.45 billion years) are often interpreted as lithified remnants of the microbial mats on early Earth, although there is no robust evidence that microbes shaped most ancient stromatolites [1]. The relationship between these mysterious rocks and biological processes at the microscale has motivated my graduate work at Caltech.

Stromatolites grow by the addition of new lamina. Microbes can contribute to the formation of lamina by trapping and binding the sediment, or by influencing calcification. For example, the main lamina-forming process in modern stromatolites is trapping and binding of the carbonate sediment by cyanobacteria and diatoms [2]. Trapping and binding was less common in the oldest stromatolites. Instead, their accretion was dominated by *in situ* precipitation of carbonates, probably due to the higher saturation state of the Precambrian seas with respect to calcium carbonate [3]. Although both *in situ* precipitated and trapped and bound structures can have similar macroscopic domical and branched shapes, these shapes could arise even in the absence of biology [4]. Furthermore, fossil microorganisms clearly indigenous to the accretionary surfaces are rare, and organic matter associated with lamina is scarce. All these factors call for the

development of process-oriented models of how microbes determine the shape of rocks and what determines the macroscopic shape of microbial communities in the first place.

I took a novel approach to develop stringent experimental criteria for the recognition of microbial biosignatures, and to test specific hypotheses about the role of microbial metabolisms in the precipitation of stromatolites. I grew model microbes with ancient metabolisms under controlled chemical conditions thought to be representative of the early Earth. Although reductionist, the strength of this approach is its ability to investigate how microbial metabolisms affect carbonate precipitation and morphology in a variety of environmental conditions that extend beyond modern environments.

Modern microbes as a probe to the ancient past

In Chapter 2, we investigated the effect that active and inactive sulfate reducing and other heterotrophic bacteria had on the nucleation of calcite under the conditions relevant for early Earth. The precipitation of carbonates in modern marine stromatolites, and by analogy, in ancient ones, had been widely attributed to the activity of sulfate reducing bacteria [5]. However, the Late Archean and Paleoproterozoic oceans (>1.6 billion years ago) apparently contained at least 20 times less sulfate, and possibly 10-100 times more dissolved inorganic carbon relative to modern seawater [6, 7]. By combining a chemical modeling study with laboratory experiments, we demonstrated that the presence of dead organic matter (dead bacteria) under these chemical conditions would have had an equal, if not larger, role in carbonate nucleation than metabolically active sulfate reducing bacteria and other heterotrophic microbes [8]. Our study suggested that abiotic mechanisms or metabolic processes other than sulfate reduction would have

stimulated the very extensive precipitation of carbonate minerals in the early oceans. The calcification within sulfate reducing biofilms was kinetically stimulated relative to the outside environment at the microscale, implying that robust morphological indicators of bacterial presence in the rock record could be expected at this scale as well [9]. The effects of G20 on calcite morphology under the chemical conditions relevant for early Earth are described in Chapter 3.

We underscored the need for caution in interpreting biosignatures by studying laboratory precipitates whose shape resembled peloids, calcite grains commonly found in the rock record. The hypotheses about the origin of peloids, typically defined as "rounded grains of homogeneous micrite", fall into two main categories: biological and abiotic. The shape and growth pattern of peloidal calcite in our abiotic experiments could be explained purely by the chemical evolution of the solution and physical processes such as stirring and gravitational settling [10]. We describe this confirmation of peloids as a poor biomarker in Chapter 4.

Sub-micron and micron-sized micropores have been tentatively interpreted as remains of microbial cells in rapidly accreting carbonate cements. We precipitated carbonate crusts in the presence and absence of G20, and produced the first laboratory evidence that similar scale microporosity did not occur in the absence of microbes. Applying a set of objective criteria established in this experiment to modern and ancient environmental samples, we found similar biogenic microporosity in some modern fast-precipitating carbonates and in an ancient stromatolite [11]. Microporosity as a biomarker is the topic of Chapter 5.

The published research from Chapters 2-5 opened many avenues for future work, some of which are discussed together with the strengths and weaknesses of our approach in Chapter 6. Chapter 7 proposes a study that would find the molecular basis of the morphology of some unique macroscopic microbial aggregates, and model the preservation of these aggregates in the rock record by precipitation experiments. Appendix A describes some ongoing and future experiments that would address the influence of light as a parameter in stromatolite morphogenesis using photosynthetic model organisms.

2. Microbial nucleation of calcium carbonate in the Precambrian

Abstract

Microbial sulfate reduction is thought to stimulate carbonate precipitation in modern stromatolites, yet whether this metabolism was important in shaping Precambrian stromatolites is unknown. Here we use geochemical modeling to suggest that the influence of sulfate reduction on the saturation index of calcite (SI) is negligible when seawater is in equilibrium with high pCO_2, as is thought for the Precambrian. Our laboratory experiments with heterotrophic bacteria in a medium mimicking Precambrian seawater chemistry show that even if sulfate reduction does not significantly change the SI, the presence of bacteria stimulates calcite precipitation over sterile controls by effectively increasing the SI over a pH range from 7.3 to 7.8. Under our experimental conditions, dead cells stimulate *in situ* carbonate precipitation equally, if not more, than active sulfate reducing bacteria. Heterogeneous nucleation of calcite by microbial cell material appears to be the driving mechanism that explains this phenomenon.

Introduction

Stromatolites are common features in the Precambrian rock record, but whether their formation was influenced by microbes to the same extent as in the Recent stromatolites is debated. While the contributions of various microorganisms and/or

microbial communities to the deposition of rare modern stromatolites have been examined [2, 5, 12], microbial contributions to the deposition of ancient stromatolites are often difficult to distinguish against a background of abiotic precipitation and to deconvolve mechanistically [1, 3, 4].

By definition, stromatolites are laminated, lithified accretionary structures that grow by the addition of new lamina. Microbes can contribute to the formation of lamina by trapping and binding the sediment, or by influencing calcification. For example, the main lamina-forming process in modern stromatolites is trapping and binding of the carbonate sediment by cyanobacteria and diatoms, although micritic carbonates precipitate in the layers of sulfate reduction [2, 5]. In contrast, *in situ* precipitation of carbonates dominated in Paleoproterozoic and Mesoproterozoic stromatolites, probably due to the higher saturation state of the Precambrian oceans with respect to calcium carbonate [13].

Sulfate reduction is a metabolism that has been associated with *in situ* carbonate precipitation in modern marine settings [14-18] and has been correlated with the formation of the micritic carbonate lamina in modern Bahamian stromatolites [2, 5]. The mechanism by which sulfate reduction could induce precipitation of calcium carbonate by an increase in alkalinity is often described by the following equations:

$$SO_4^{2-} + 2CH_2O \rightarrow HS^- + 2HCO_3^- + H^+$$

$$Ca^{2+} + HCO_3^- \rightarrow CaCO_3(s) + H^+$$
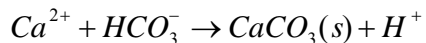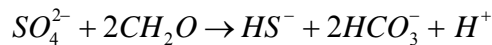
However, it is unclear whether this mechanism would drive calcite precipitation in oceans that are well buffered by high concentrations of dissolved inorganic carbon (DIC), inferred for the early Proterozoic oceans. Here we consider how sulfate reducing

bacteria (SRB) stimulate *in situ* carbonate precipitation under environmental conditions relevant for the Precambrian, through modeling and laboratory studies of *Desulfovibrio desulfuricans* strain G20.

Materials and Methods

Growth medium and conditions. We used *D.desulfuricans* strain G20 as a model organism. To test whether the effect of microbes on calcite precipitation was specific to SRB, we used a phylogenetically distant Gram-negative bacterium *Escherichia coli* HB 101, a facultative anaerobe that colonizes human gut and cannot reduce sulfate. G20 was grown in modified, bicarbonate-buffered Postgate medium on 0.5 mM Na-sulfate and 10 mM Na-lactate as the electron acceptor and donor, respectively [19]. The basal medium contained: 8 mM $MgCl_2$, 20 mM NH_4Cl, 0.5 mM KH_2PO_4, 0.2 g/l yeast extract. The basal medium was boiled under N_2, autoclaved and cooled under N_2/CO_2. 1ml/l SL 12-B trace element solution and 1 ml/l Pfennig vitamin solution, 10 mM Na-lactate, 0.5 mM Na_2SO_4, 10 ml/l 2.5% cysteine-HCl, 7.6 ml/l 8% Na_2CO_3 and 70 ml/l 1 M $NaHCO_3$ were added from sterile stock solutions, the pH was adjusted by 10 N NaOH to 7.4 -7.5, and the medium was left to equilibrate with an atmosphere of 80% N_2, 15% CO_2 and 5% H_2 for at least one day. Finally, the medium was filter-sterilized by a 0.2 μm filter. Escherichia coli strain HB101 was grown in the same medium with an additional 2 mM Na-fumarate as the electron acceptor. Both organisms were grown anaerobically under an atmosphere of 80% N_2, 15% CO_2 and 5% H_2.

Precipitation experiments. 0.5 ml of early stationary phase bacteria (cell density 5 x 10^7 cells/ml) was centrifuged to remove the liquid phase. The bacteria were then inoculated into 0.4 ml of the fresh culture medium from 8-well LabTek$^®$ (NalgeNunc International) chambered coverglass culture dishes with coverslip bottoms. After inoculation, $CaCl_2$ was added to sterile controls and cultures to 20 m*M* final concentration. Filter-sterilized nigericin was added to inhibit the cultures in two wells to the final concentration of 0.04 m*M*. These concentrations of nigericin completely inhibit the growth of G20 (data not shown). The UV treatment consisted of exposing bacteria to UV light on a Foto/Convertible™ transilluminator (Fotodyne Incorporated). Plate counts confirmed that the number of viable cells in UV-treated cultures was at least 10^{-6} times lower than in the original stock. The incubation time was 15 to 20 hours at 25°C (relative comparisons were made only between cultures incubated for the same amount of time). The amount of precipitate was determined by taking transmitted light micrographs of at least10 different fields of view using a Zeiss Axiovert S100 microscope. We measured the area covered by precipitates using MetaMorph$^®$ (Universal Imaging Corporation™). When the crystal sizes varied (such as in the experiment with different initial pH values), their volumes were estimated by comparing them to a crystal with a defined unit volume. The relative volume for each experiment was then calculated by averaging the total volume in a given field of view for 10 independent fields.

Geochemical modeling. Chemical parameters such as supersaturation and concentrations of chemical components in the medium were calculated using MINEQL+ (Environmental Research Software). We assumed a closed system (before and after the loss of sulfide). The model solution had basal ion concentrations equal to our freshwater culture medium

(see above) but with 10 mM CaCl$_2$ and 20 mM Na$_2$SO$_4$ (i.e., closer to their respective concentrations in present-day seawater).

Results and Discussion

Modeled Effect of Sulfate Reduction on Calcite Saturation

To predict the effects of sulfate reduction on calcite precipitation in media with initial concentrations of DIC ranging from the present day (2 mM) to putative Precambrian conditions (72 mM), we modeled the saturation index (SI) of calcite before and after sulfate reduction (Fig. 1). SI is defined as log(IAP/K$_s$), where IAP is the ionic product of calcium and carbonate and K$_s$ is the solubility constant of calcite. An increase in the SI after sulfate reduction reflects a higher potential for calcite precipitation. Conversely, if the SI decreases after sulfate reduction, calcite will be less likely to precipitate. The change in SI depends on the amount of sulfate reduced, the initial concentration of DIC, and the processes that remove sulfide and carbon dioxide from solution.

At relatively low rates of sulfate reduction similar to those measured in modern Bahamian stromatolites [20], we estimate that approximately 0.5 mM sulfate could be reduced in 24 h in the layer of maximum sulfate reduction. If all metabolic products were to stay in solution over this time period, our model predicts that both the pH and the SI will decrease regardless of the initial concentrations of DIC (Fig. 1a). If we assume ten times more sulfate is reduced over the same time period, we expect SI to increase only when DIC is low, as is the case for present-day seawater (Fig. 1a).

For any concentration of DIC, it is also possible for sulfate reduction to increase the SI if we assume that CO_2 and H_2S leave the solution by outgassing, or if sulfide reacts with Fe(III) minerals [18]. If sulfide reacts with Fe(II), however, the pH will decrease and reduce the SI: $Fe^{2+} + H_2S \rightarrow FeS(s) + 2H^+$. Because reactions with iron will rapidly remove sulfide from solution, for the purpose of our model, we have assumed that all sulfide is removed instantaneously through such reactions, enabling us to neglect the slower dynamics of outgassing.

Based on these assumptions, our model predicts that the reduction of 0.5 mM sulfate will increase SI at most by 0.3 log units in a poorly buffered aqueous environment (2 mM total DIC) when all sulfide is removed. Even if sulfate reduction were to occur at lower concentrations of organic acids, as is likely the case in modern stromatolites [5], this would not affect the difference in SI before and after sulfate reduction (data not shown). The greater the amount of reduced sulfate, the greater the increase in SI and the potential for calcite precipitation in modern seawater (Fig. 1b). In well-buffered systems that are supersaturated with respect to calcium carbonate, even if all sulfide is lost from solution, the increase in SI will be negligible (Fig. 1b). Because sulfate concentrations in the Archean and early Proterozoic are thought to be less than 0.5 mM [21-23], and pCO$_2$ is considered to have been much higher than today [24], we believe that the modeling results shown in Fig. 1b rule out a significant role for sulfate reduction in stimulating calcite precipitation at that time.
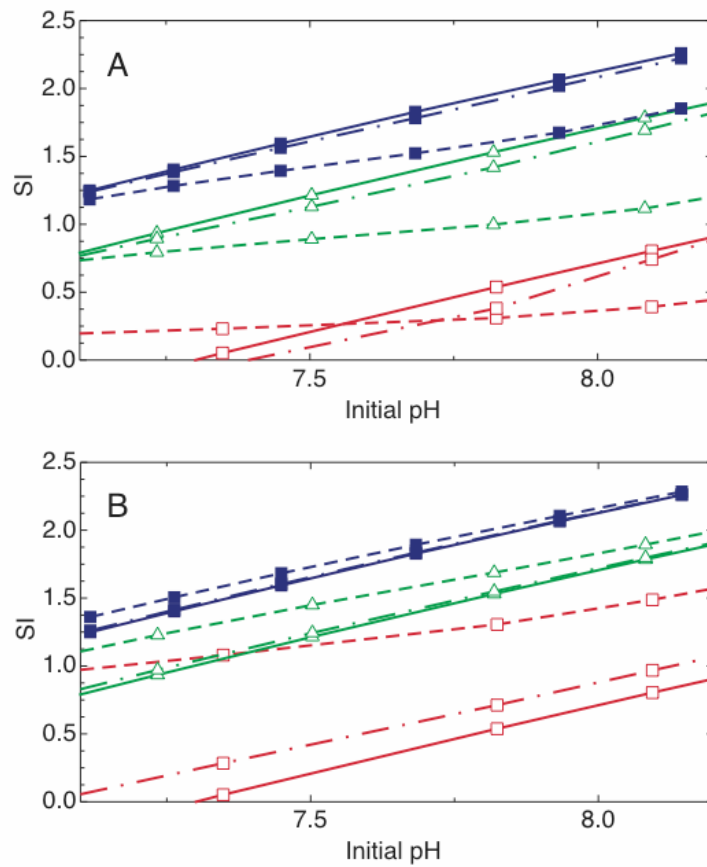
Figure 2-1   A: SI of calcite calculated before (solid line), after reduction of 0.5 mM SO$_4^2$ with lactate (dot-dashed line), and after reduction of 5 mM SO$_4^{2-}$ with lactate (dashed line) assuming that all sulfide stays in the medium. SI is calculated for the initial dissolved inorganic carbon concentrations of: 2 mM (red), 22 mM (green) and 72 mM (blue). B: The same as above but assuming that all sulfide produced by sulfate reduction is removed from the system.

Effects of Bacteria on Calcite Precipitation

Because our geochemical modeling does not predict a significant effect of sulfate reduction on SI, we hypothesized that sulfate-reducing bacteria could stimulate calcite precipitation by a mechanism other than sulfate reduction. To test this, we used *D. desulfuricans* G20 as a representative SRB to determine how its presence affected calcite precipitation under conditions that mimicked Archean and early Proterozoic seawater chemistry. At the beginning of our precipitation experiments, the culture medium was almost 100 times supersaturated with respect to calcite. Calcite crystals (identified by X-ray diffraction) precipitated both in the uninoculated (sterile) controls and G20 cultures. A characteristic crystal is shown in Fig. 2a. These experiments consistently showed that about 82% more calcite formed in the presence of G20 than in the sterile controls at initial pH 7.4 (Table 1).

Table 2-1 DIFFERENCE IN THE VOLUME OF PRECIPITATE
BETWEEN BACTERIAL CULTURES AND STERILE CONTROLS

Condition	Difference (%)		
Sulfate reducer G20 in "freshwater" medium[*]			
G20 uninhibited	82	±	17
G20 inhibited by UV[†]	138	±	8
G20 inhibited by nigericin[§]	137	±	18
G20 outer membranes	53	±	15
Sulfate reducer G20 in "saltwater" medium[#,**]			
G20 uninhibited	41	±	1
G20 inhibited by UV[†]	77	±	18
Anaerobically grown *E.coli* HB101[#]			
HB101 uninhibited	18	±	11
HB101 inhibited by UV[†]	54	±	19

Note: Differences shown are averages of at least two independent experiments, with volumes determined from at least 10 different fields of view. Uninhibited and inhibited cultures were incubated at the same initial cell density.
[*]Determined at initial pH 7.4
[†]UV is ultraviolet light.
[§]Nigericin did not stimulate precipitation in the absence of bacteria.
[#]Determined at initial pH 7.5.
[**]Saltwater medium contained an additional 20 g/L NaCl and 1.4 g/L $MgCl_2$

To determine whether metabolically inactive G20 could enhance carbonate precipitation, we inhibited its metabolism chemically (by adding nigericin) and physically (by exposing it to ultraviolet (UV) light). Nigericin has been shown to collapse the membrane proton gradient in sulfate-reducing bacteria [25, 26], whereas UV light kills cells by damaging DNA and preventing cell division. We observed significantly more precipitate at pH 7.4 relative to sterile controls in metabolically inactive cultures (Table 1). In contrast to our results, Chafetz and Buczynski [27] observed lithification in modern microbial mats only when living bacteria (presumably heterotrophs) were present. In keeping with our modeling results (Fig. 1), we suggest that these differences are due to metabolically induced changes in SI given the lower buffering capacity of modern seawater.

Although we used G20 as our model species, stimulation of calcite precipitation is not specific to sulfate reducing bacteria. *Escherichia coli* HB101, a bacterium that colonizes the human gut, also stimulates precipitation of calcite when growing on fumarate instead of sulfate and even more so when inhibited by UV (Table 1). An increase in heterogeneous nucleation in G20 and HB 101 cultures is probably due to the binding and accumulation of metal ions by negatively charged carboxylate and phosphoryl groups on bacterial surfaces [28, 29]. As shown by Mera et al. [30], cell walls of the Gram-positive bacterium *Bacillus subtilis* bind more metal when the proton gradient across the cell membrane is artificially collapsed. The release of charged compounds through compromised cell membranes of the inhibited organisms into the extracellular medium could additionally stimulate mineral precipitation.

Having experimentally confirmed that bacteria stimulate calcite precipitation by mechanisms other than metabolic activity, we sought to determine the range of pH conditions over which this stimulation could be measured. Assuming a constant radius of calcite nuclei, the free energy of homogeneous nucleation, ΔG, increases linearly with SI:

$$\Delta G \propto SI \tag{1}$$

The nucleation rate, J, increases exponentially with the free energy of nucleation:

$$J \propto \exp(\Delta G) \tag{2}$$

SI (as defined above) increases linearly with pH. J will therefore increase exponentially with SI and pH [31]. Indeed, the relative difference in the amount of precipitate between inhibited cultures of G20 and sterile controls depends on the initial pH of the medium and is measurable in the pH range from 7.3 to 7.8 (Fig. 2b). This range is consistent with the estimated pH range of the Precambrian oceans [13]. When the initial pH of the medium was below 7.2, we did not observe any mineral grains in either G20 cultures or controls, even though the medium was more than 30 times supersaturated with respect to calcite. The absence of precipitation at lower pH values is probably due to kinetic inhibition of nucleation in our medium. The critical value of SI needed to start mineral precipitation in our experiments is consistent with critical SI values of about 1 (10-fold supersaturation) that have been observed in modern soda lakes [32]. When the initial pH was 8.0, the amount of precipitate in the control medium and G20 cultures was the same within the experimental error (Fig. 2b).
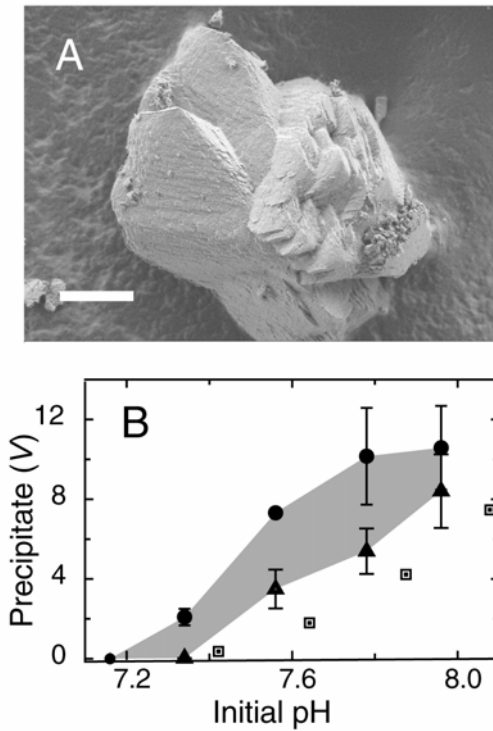
Figure 2-2   A: Scanning electron micrograph of a representative calcite crystal precipitated in G20 cultures at pH 7.5. The image was obtained on a LEO1550 VP field emission scanning electron microscope operating at 10 kV. Scale bar: 20 μm. B: Relative volume (*V*) of calcite in nigericin-inhibited G20 cultures (dots) and sterile controls (triangles). Filled boxes: predicted volume, assuming it is proportional to the homogeneous nucleation rate that is proportional to SI as calculated by MINEQL+. Shaded area shows the range of measurable differences between biologically influenced precipitation and sterile controls. The results shown are averages of two independent experiments.

A comparison of the theoretical rate of homogeneous calcite nucleation with our experimental data suggests that bacteria affect calcite formation mainly kinetically, by increasing the rate of heterogeneous nucleation. In other words, metabolically inactive G20 effectively increases the SI by at least 0.3 SI units over sterile controls. We estimate the effective difference in SI by assuming that the measured volume of precipitate is linearly proportional to the nucleation rate: $V \propto rate$ (Fig. 2b). Because the nucleation rate depends exponentially on the SI (Equation 2), the logarithm of the ratio of precipitate volumes in G20 cultures and sterile controls defines the effective difference in SI: $\log \frac{rate_{G20}}{rate_{control}} = SI_{G20} - SI_{control}$. Although this is only a first-order approximation, the effective increase in SI appears to be at least as great as the maximum modeled increase in SI due to sulfate reduction under conditions relevant for the Precambrian (Fig. 1).

Summary

In contrast to field studies of lithification in modern stromatolites, our results demonstrate that sulfate reducing bacteria can influence the rates of calcium carbonate precipitation by mechanisms that do not require metabolic activity. Given the proposed composition of Archean and early Proterozoic seawater, heterotrophic sulfate reduction thus is not likely to have had a significant effect on calcification. Rather, microbial viability may have been a more important parameter in determining the rates of heterogeneous calcite nucleation. Dying cells remaining in the lower portions of upwardly moving microbial communities may have been the sites of most rapid carbonate nucleation in ancient stromatolites. In modern environments, microbial cell

death may also significantly contribute to lithification, although metabolic effects are more likely to dominate.

3. Microbial kinetic controls on calcite morphology in supersaturated solutions

Abstract

Recognizing microbial imprints in the morphology of calcium carbonate is challenging. To better define criteria for this purpose, we have analyzed the influence of sulfate-reducing bacterium *Desulfovibrio desulfuricans* strain G20 on the morphology of calcite in supersaturated solutions that contain a high level of dissolved inorganic carbon (DIC). G20 does not induce large shifts of pH or alkalinity under these conditions, but its uptake of millimolar sulfate and lactate decreases the number of anhedral crystals and stimulates growth of subhedral spar crystals relative to the abiotic controls. In addition, organic compounds associated with the basal growth medium, purified exopolymeric substances produced by G20 and lypopolysaccharide, stimulate the growth of anhedral crystals and crystals with rounded edges at low supersaturation index (SI) of calcite. The effect of organic compounds is reduced at higher SI, where rhombohedral habits dominate. Our results suggest that the local production and uptake of kinetic inhibitors within microbial biofilms are important controls on calcite morphology in supersaturated solutions.

Introduction

Finding unique microbial morphological biomarkers in the most ubiquitous calcium carbonate minerals (calcite and aragonite) is a challenging but essential step toward understanding the parallel evolution of life and the environment on Earth [1], and beyond [33]. Microbial signatures in these minerals are often only putative because a variety of biological and abiotic processes can readily alter the solution chemistry and result in similar crystal shapes.

In inorganic solutions that contain only calcium and carbonate salts, the amount and the morphology of calcium carbonate minerals depend on the supersaturation index (SI) of these minerals and their precipitation rate [34-36]. The supersaturation index [SI] of a mineral is a measure of how much a solution departs from the thermodynamic equilibrium with respect to the precipitation of that mineral [37]. The SI of calcite is defined as $\log(IAP/K_s)$, where IAP is the ionic product of calcium and carbonate and K_s is the solubility constant of calcite ($K_s = 10^{-8.48}$). The same analysis applies to other polymorphs of calcium carbonate such as aragonite, taking into account their different solubility constants (K_s for aragonite is $10^{-8.33}$). Most natural solutions contain ions such as magnesium, sulfate, and phosphate that act as kinetic inhibitors of calcite precipitation and alter its morphology [36, 38-40].

Multiple microbial mechanisms can influence the amount and shape of calcium carbonate minerals in solutions that are not highly supersaturated with respect to calcium carbonate (e.g., modern seawater, and the water in marine sediments, caves, and soils). Microbes can change the SI of calcium carbonates, take up and secrete various kinetic inhibitors, or bind calcium and magnesium ions on their negatively charged outer

surfaces [5, 14, 15, 41-48]. In highly supersaturated environments that contain a lot of dissolved inorganic carbon (DIC) like soda lakes and hot springs, microbial biofilms can leave morphological signatures [32, 49-51], although the amount of precipitated carbonate is not predicated upon metabolic shifts of SI [8, 52]. Some of these signatures have been confirmed by laboratory experiments [11], but how various microbes interact with carbonate minerals in the presence of high DIC deserves more experimental attention.

Investigating the effects of sulfate reduction on calcite precipitation in a medium with high initial SI, high DIC, and little sulfate, we noticed that calcite crystals in the cultures of metabolically active *Desulfovibrio desulfuricans* strain G20 had different shapes than the crystals in the G20 growth medium without bacteria. Because carbonate rocks from the early Earth apparently precipitated from much more supersaturated solutions that contained little sulfate relative to the modern-day oceans [1, 21, 23, 53], little sulfate and high DIC in our experimental solutions are relevant not only for modern-day high-DIC environments but also for the early Earth. Here we describe some of the mechanisms by which G20, its cellular fractions, and its metabolites can alter calcite morphology as an initial step in the development of a model system in which to study interactions between biofilms and accreting carbonate minerals. Our objective is to understand the relative importance of inorganic versus microbial processes that influence the formation of calcite crystal habits in solutions where substantial precipitation occurs regardless of microbial activity.

Materials and Methods

Bacterial strain, culture medium and experimental conditions. D. desulfuricans strain G20 was generously provided by Judy Wall (University of Missouri). All precipitation experiments were carried out under an anaerobic atmosphere of 0.8 atm N_2, 0.15 atm CO_2, and 0.05 atm H_2 in bicarbonate-buffered anaerobic G20 basal medium at 25°C. The composition of the basal medium is described in Table 1. The SI of our solutions was changed either by changing the pH of the medium (thus changing the amount of carbonate ion) or by modifying the activity of the calcium ion. To that end, we either established the pH from 6.8 to 8.0 in aliquots of the basal medium by adding 1 N HCl or 10 N NaOH or added $CaCl_2$ to aliquots of the basal medium to a final concentration from 5 to 20 mM at a constant pH (7.5). While these pH values are lower than some estimates of the marine pH in the Precambrian (pH > 9) [52], they are consistent with the estimates of Grotzinger and Kasting [13], and the high pCO_2 inferred by Ohmoto, Watanabe et al. [7]. 20 mM calcium concentration is high relative to the modern seawater (10 mM), but calcium concentrations even higher than 20 mM are consistent with calcium levels required to support the calcification of cyanobacterial filaments at various times in the Earth's history [52].

The standard G20 growth (and precipitation) medium contained 1 mM sulfate and 3 or 10 mM lactate (further specified in the text). Although much higher concentrations of sulfate and lactate (~ 20 mM and ~ 50 mM, respectively) are commonly used to grow sulfate-reducing bacteria, we used these low concentrations in keeping with the low sulfate concentrations inferred for the Precambrian oceans [21, 23], and our previous work [8]. Microscopic counts of cells stained by 4',6-Diamidino-2-phenylindole (DAPI)

(Sigma-Aldrich) confirmed that biomass doubling could occur even with 1 mM sulfate in the medium.

To investigate the effect of organic additives in the basal medium on calcite morphology, we made a solution that contained all of the inorganic constituents (Table 1) but lacked the organic compounds (yeast extract, vitamins, cysteine, and lactate). We conducted precipitation experiments in aliquots of the inorganic basal medium whose initial pH varied from 6.4 to 8.2. This experiment was repeated twice.

To obtain a dense bacterial inoculum for the precipitation experiments, G20 was grown with 3 mM Na-sulfate (growth-limiting concentration) and 10 mM Na-lactate as the electron acceptor and donor, respectively. The UV treatment consisted of exposing bacteria to UV light for 5 minutes on a Foto/Convertible™ transilluminator (Fotodyne Incorporated). To assay the metabolic activity of UV-treated cells, we measured lactate and acetate concentrations in untreated and UV-treated G20 cultures (with 3 mM initial sulfate and 10 mM lactate) by Waters 717plus Autosampler HPLC (high-performance liquid chromatograph) with an Aminex® HPX-87H column by BioRad.

Table 3-1 The composition of the G20 culture medium during a 20 h precipitation experiment

Component	Initial G20 growth medium	G20 medium after 20 h	Comment
Inorganic			
pH	7.52 ± 0.01	7.51 ± 0.01	
Alkalinity (meq)	80 ± 1	77 ± 1	Measured by Gran-titration using 0.8 M H_2SO_4 (average of three separate tubes).
Ca	20.1 ± 0.8	18.9 ± 0.2	Measured by ICP-MS (average of three separate tubes). The same decrease in total Ca was observed in another independent experiment.
SI	2.067	2.036	The SI was modeled by MINEQL+, assuming an equilibrium with 0.15 atm CO_2 and titrating by LiOH to obtain the measured pH (the pH of the actual medium was adjusted by NaOH). The measured changes in pH, Ca, and C-alkalinity correspond well to the expected changes in an open system modeled by MINEQL+. The pH of the model medium was calculated by imposing electroneutrality condition.
SO_4	1	ND	ND: Known concentrations (in mM, unless stated otherwise) were added to the basal medium and not measured afterward.
Cl	56.5	ND	Only Cl that was added with basal salts, more HCl was added to adjust the pH.
K	0.5	ND	
Mg	8	ND	
Na	98	ND	Only Na that was added with basal salts, more NaOH was added to adjust the pH.

NH$_4$	0.5	ND	
PO$_4$	0.05	ND	
SL12-B mineral solution (ml/l)	1	ND	http://www.dsmz.de/media/med028.htm
Organic			
acetate	0	ND	
lactate	10	ND	
yeast extract (g/l)	0.15	ND	
cysteine-HCl	1.4	ND	
Vitamin solution (ml/l)	1	ND	4 mg 4-aminobenzoic acid, 1 mg D(+)-biotin, 10 mg nicotinic acid, 5 mg Ca-D(+)-pantothenate, 15 mg pyridoxamine dihydrochloride, 10 mg thiaminium dichloride, and 5 mg cyanocobalamine per 100 ml nanopure water

Extraction of G20 cellular fractions. We extracted the exopolymeric substances (EPS) produced by G20, its outer envelopes, and the lypopolysaccharide (LPS) fraction of the outer cell membrane to compare and contrast their *in vitro* effects on calcite morphology.

To precipitate EPS, we grew 1 liter of G20 with 20 mM Na-sulfate and 50 mM Na-lactate to a cell density of 1.5 x 10^8 cells/ml. The early stationary culture was then spun at 10,000 *g* at 4°C, the supernatants were mixed with 3 volumes of cold isopropanol (4°C) and left to precipitate for 3 days at 4°C [54]. Precipitated EPS were dialyzed for 48 hours with nanopure water in a SpectraPor dialysis membrane with MS3500 molecular cutoff (Spectrum Laboratories, Inc.). Dialyzed EPS were lyophilized and stored at –80°C.

To isolate the outer membranes from cultures in early stationary phase (1.5×10^8 cells/ml), we centrifuged 1 l of cells in 0.05 M HEPES (pH 7.5) at 10,000 g at 4°C for 30 minutes. Cell suspension (3 g/10 ml of 0.05 M HEPES) was then incubated on ice for 2 hours and centrifuged at 5,000 g and 4°C for 30 minutes [55]. G20 was resuspended in 10 ml of 0.05 M HEPES with added 50 µg/ml DNAse (Roche), 1mM $MgCl_2$, and 10 µg/ml RNAse (Roche). The cell suspension was kept on ice and sonicated for 5 minutes in 30 s pulses. The unbroken cells were separated from the lysate by centrifugation at 7,000 g at 4°C for 20 minutes. The cytoplasmic extract was then separated from the cell membranes by ultracentrifugation at 45,000 rpm (SW60 swinging bucket rotor on a Beckman Ultracentrifuge) at 4°C [56] and the membranes were stored at –20°C. LPS was extracted from DNAse-, RNAse-, and lysozyme-treated (Sigma) membrane fractions according to Gerhardt et al. [56], lyophilized, and stored at –20°C. The absence of RNA and DNA in the membrane fractions was assayed by measuring the absorbance at 260 and 280 nm during successive rinses of the membrane fractions in nanopure water on a Beckman DU7400 spectrophotometer.

The protein content of lyophilized EPS was assayed by the Bio-Rad Protein Assay based on the method by Bradford [57]. The amount of neutral carbohydrates in EPS was measured by the H_2SO_4 - phenol method using glucose as standard [56]. The amount of uronic acids was determined with *m*-hydroxydiphenyl in H_2SO_4/sodium tetraborate solution using D-glucuronic acid as the standard [58]. Nucleic acid content in EPS was assayed qualitatively by staining the EPS extract with ethidium bromide in a 2% agarose gel.

Precipitation experiments.   To study the influence of G20 metabolism on calcite morphology, 0.5 ml of untreated or UV-treated late exponential phase bacteria (cell density 5 x 10^7 cells/ml) were centrifuged to remove the liquid phase. Washed bacteria (either untreated or UV-treated) were resuspended in the fresh culture medium (1 ml original culture per 0.8 ml fresh medium) and transferred into 8-well LabTek$^®$ (NalgeNunc International) culture dishes with coverslip bottom (0.4 ml/well). The same amount of sterile medium without bacteria was added to separate wells as a control. In the experiments without bacteria, we added various chemicals or cellular fractions to the sterile medium in the same culture dishes. Finally, $CaCl_2$ was added to each well containing the precipitation medium (with or without cells) to a 20 mM final concentration. The growth of calcite crystals was investigated after 20 hours by transmitted-light microscopy. All precipitation experiments were performed at least twice under each described condition. The calcium concentration was measured by inductively coupled plasma mass spectrometry (ICP-MS) in dilute filtered samples (100 l medium/10 ml 1% HNO_3) in triplicates.

Transmitted-light, confocal, and scanning electron microscopy.

The morphology of precipitates was examined by taking transmitted-light micrographs from at least 10 different fields of view using a Zeiss Axiovert S100 microscope. The crystals were point-counted to obtain percentages of specific morphologies. The crystals with intermediate morphologies were assigned to both end-member morphological classes. All percentages were estimated from at least two independent experiments.

Fluorescence confocal microscopy of G20 biofilms was performed on an inverted Zeiss Pascal LSM (laser scanning microscope). The biofilm samples were prepared for imaging as follows: biofilms were grown in the growth medium for 20 h in 8-well LabTek® (NalgeNunc International) culture dishes with coverslip bottom, the medium was then replaced by 0.5 M HEPES buffer, 2 μl dye (Live Dead® BacLight™ by Molecular Probes) per 0.5 ml buffer, and the biofilms were incubated in the dark for 15 minutes before imaging. The fluorescence of the samples was excited at 488 nm.

EPS and bacteria were stained by the method of Allison and Sutherland [59].

C-coated precipitates were imaged by a LEO1550 VP field emission scanning electron microscope operating at 2 kV at a 5 mm working distance.

Mineral analysis. The crystal structure of the precipitates was determined by X-ray diffraction using a Scintag diffractometer with Cu K (λ = 1.5405 Å). The crystals were washed with 10% bleach and rinsed in nanopure water before analysis. The crystallinity of samples was determined by looking at the full width of the 104 Bragg calcite peak at half maximum (FWHM) [60].

Chemical Modeling. Supersaturation index (SI) and calcium and carbonate activity coefficients in the growth medium (see above) were calculated using MINEQL+ (Environmental Research Software), assuming an open system in equilibrium with 0.15 atm CO_2. The appropriate pH value was established by numerical titration by LiOH or HCl. The composition of the modeled medium (Table 1, but without trace metals, vitamins, yeast extract, and cysteine) was adjusted according to the laboratory experiments (sulfate or lactate concentrations, etc.). The calcite saturation constant used by the program is $K_s = 10^{-8.48}$ and the software calculated the ionic strength of the

medium from the supplied concentrations of the ions in the medium, adjusting the equilibrium constants accordingly.

Results and Discussion

Calcite Morphology in the Presence of Bacteria

X-ray diffraction analyses of the powdered samples confirmed that calcite constituted at least 95% of the calcium carbonate precipitate in G20 basal medium under all tested conditions. Comparing active G20 and sterile controls (without any bacteria) in two independent experiments, we found that $18 \pm 2\%$ of the total crystals in G20 cultures were truncated rhombohedra with stepped faces as opposed to $3 \pm 1\%$ in sterile controls (Fig. 1A; also see Fig. 2J for an SEM of a representative crystal). Under the transmitted light, the edges of the {04.1} rhombohedra in G20 cultures also appeared more rounded relative to the corresponding crystals in sterile controls (Fig. 1A, B, circled). Sterile controls, in turn, contained a higher percentage of anhedral crystals or complex twin aggregates of crystals with stabilized {10.0} faces (Fig. 1B and Fig. 2E-G).

To test whether the observed changes were induced by G20's active metabolism, we incubated UV-inhibited G20 at the same cell density as the living G20 and compared the shapes of calcite at the end of the precipitation experiment. The UV-treated cells consumed only 0.79 ± 0.03 mM lactate in 20 h. Because the reduction of 1 mole of sulfate is coupled with the oxidation of 2 moles of lactate, it follows that the UV-treated cells consumed less than 0.5 mM of the available sulfate during the experiment. Lactate and acetate concentrations in the untreated G20 cultures, on the other hand, indicated that all available sulfate was consumed in 20 h. Thus, the UV treatment significantly

decreased the ability of G20 to carry out dissimilatory sulfate reduction. Plate counts confirmed that the number of viable cells in UV-treated cultures was at least 10^6 times lower than in the original stock, i.e., there were fewer than 10^3 viable cells per culture well in UV-treated cultures. Given that G20 cell density increases about 10 times in 20 h (the duration of the precipitation experiment), and that morphological influence of G20 is discernible only at cell densities higher than 10^7 cells/ml, even if growth occurs in the UV-treated cultures, the effects of less than 10^4 cells/ml during the experiment would not be noticeable. Indeed, we found that the precipitate formed in the presence of UV-inactivated bacteria was similar to that in the sterile controls (Fig. 1C).
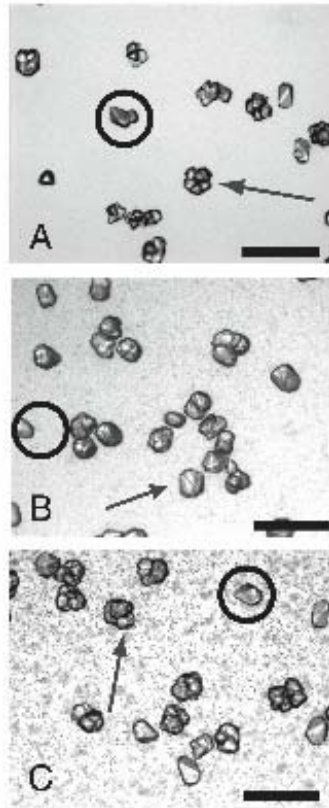
Figure 3-1   Calcite morphology in the presence of metabolically active G20 differs from that in sterile and UV-inhibited controls. The arrows in all images indicate typical rhombohedral crystals and twins. The circles in all images indicate spar crystals with {04.1} faces. A) Sterile control without any cells. The twins appear to have grown by reflection on {10.4} plane (arrow), and the rhombohedral spar crystals have sharp edges (circle). B) Active G20. Many {04.1} rhombohedra (arrow) have stepped faces, and all crystals have more rounded edges (circle).   C) Twin and spar crystals in UV-inhibited G20 cultures are similar to the crystals in sterile controls A). The dark gray aggregates in the background of Parts B and C are bacteria. The scale bar in all images is 200 μm.
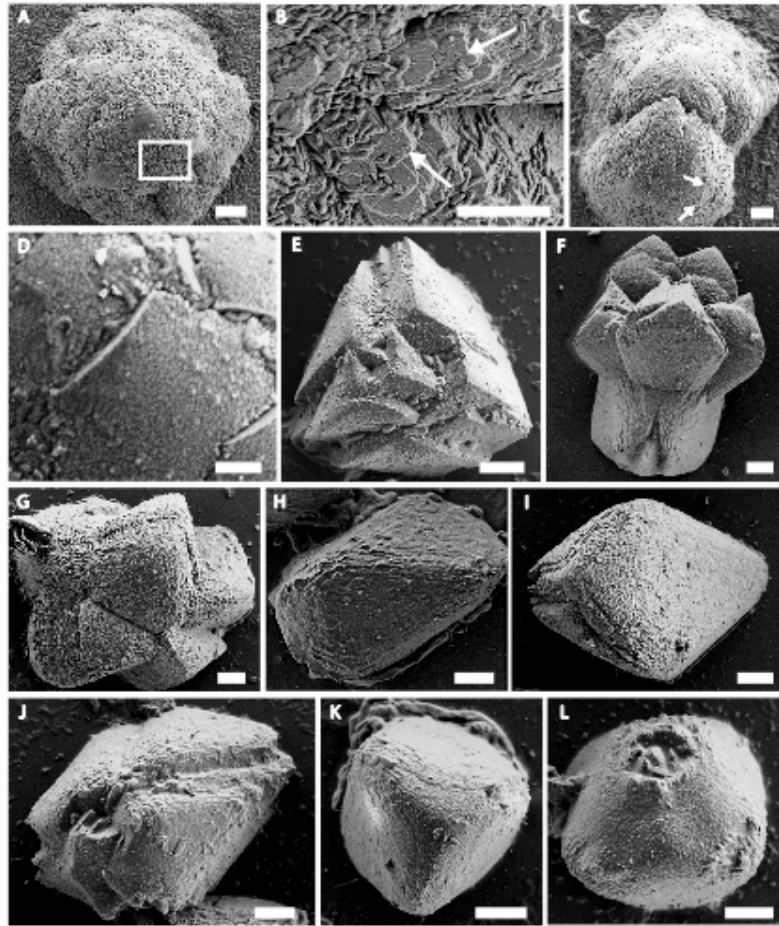
Figure 3-2 Scanning electron micrographs (SEMs) of representative calcite crystals precipitated in the presence of organic compounds in the order of increasing SI. A) Cauliflower-like hemispherical precipitate at low SI ($0.5 \leq SI \leq 1$) formed by aggregates of bladed calcite with uneven edges (rectangle shows the area of the close-up in 2B) and stepped curved planes. B) Close-up of Fig. 2A. Bladed calcite crystallites with irregular edges stabilized by organic molecules at low SI. The crystallites are oriented in the same direction only locally but do not aggregate into a recognizable crystal face (arrows). The small, elongated features are G20 cells. The scale bar is 5 μm. C) Double hemispherical precipitate at $0.5 \leq SI \leq 1$. The arrows indicate curved planes (see a close-up in Part D). D) Curved, stepped planes are also stabilized by organic additives in the basal medium at

low SI. The scale bar is 3 μm.   E) About 10% of the crystals at low SI had stabilized {10.0} faces. F) Twin (most likely on {01.2}) with stabilized {10.0} faces and negative faces (arrow) that forms at $1 \leq SI \leq 1.5$. G) Twin (probably on {10.4}) of rhombohedral crystals, $1 \leq SI \leq 1.5$. H) Truncated spar crystal with stabilized {04.1} faces, $1.2 \leq SI$. I) Elongated rhombohedron with stepped growth along {10.0}, $1.5 \leq SI \leq 2.0$. J) Truncated spar crystals with stabilized and stepped {04.1} faces form almost 50% of the precipitate at $2.0 \leq SI$. K) Rhombohedral habits with a smaller aspect ratio than in Part I form at $2.0 \leq SI$. L) Truncated rhombohedral habit with stabilized {10.0} faces. The scale bar in all images except for Parts B and D is 10 μm.

To understand how active G20 induced these changes in calcite morphology, we wanted to establish whether we could induce comparable changes by varying some basic chemical parameters in the growth medium (SI and the presence of organic molecules and major metabolites).

Effects of Supersaturation, Sulfate, and Lactate on Calcite Morphology in the Presence of Bacteria

SI As a Control on Calcite Morphology.   Calcite morphology in G20 growth medium is strongly affected by SI. Figure 2 captures the most representative crystal shapes precipitated in the G20 basal medium, although we observed a small number of crystals with intermediate morphologies as well. Overall, as SI increased, the total number of crystals increased and their grain size decreased because of an increase in the number of crystal nuclei. Distinctly anhedral large crystals formed at the lowest pH values ($0.5 \leq SI$

≤ 1) (Fig. 2A-D). They were roughly hemispherical (because of growth on a flat glass surface), created by stepped aggregates of bladed crystals with irregular edges (Fig. 2A, B) and curved stepped surfaces (Fig. 2C, D). At low to intermediate SI ($1 \leq SI \leq 1.5$), less than 10% of the crystals were distinctly anhedral. Instead, we found stabilized {10.0} faces (Fig. 2E-G), negative faces (Fig. 2F), and twinned aggregates (Fig. 2F, G). About 20% of the total crystals in this SI range were rhombohedra, either truncated, with stabilized {04.1} faces (Fig. 2H), or elongated, with recognizable {10.0} faces (Fig. 2I). Truncated rhombohedral grains with prominently stepped {04.1} faces (Fig. 2J) or with {10.0} faces (Fig. 2K,L) dominated at even higher initial SI ($SI \geq 2.0$). At highest SI (SI ≥ 2.5), most precipitate consisted of intergrown aggregates of {10.0} and {04.1} rhombohedral grains. We observed this morphological trend both when we varied the total calcium concentration at a constant pH of 7.5, and when we varied the pH at a constant calcium concentration of 20 mM. Figure 3 shows the stability diagram for the three major morphological classes (in the presence of G20).
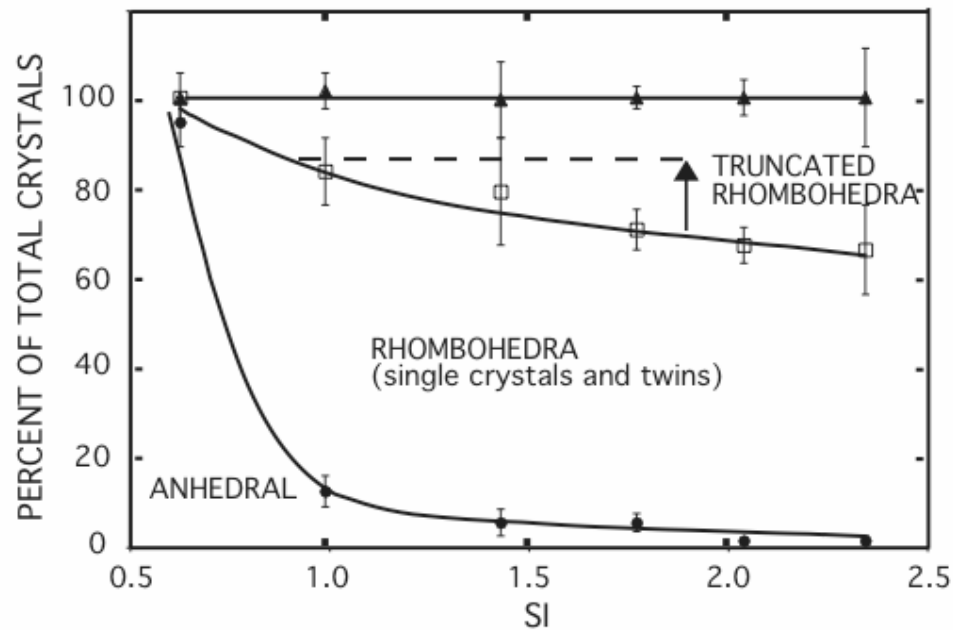
Figure 3-3   Cumulative stability diagram of characteristic calcite habits observed in

the basal medium (in the presence of organic compounds, lactate, sulfate, and G20). For

any SI the total percentages of crystals add up to 100%, and the lines delineate the

fraction of this total that belongs to any particular crystal habit. The relative percentages

of crystals habits were obtained by counting the crystals from ten independent fields of

view at each SI in two independent experiments. The average percentages of the three

major classes measured in two independent experiments are plotted as symbols: anhedral

crystals (solid circles), rhombohedral crystals with prominent {10.0} faces (hollow

rectangles), and truncated rhombohedral crystals with prominent {04.1} faces (solid

triangles). The error bars show the data range. The solid lines drawn through the points

mark the regions of stability of each major class. As the SI increases, the anhedral habits

give way to rhombohedra and truncated rhombohedra. The arrow shows the observed

difference in {04.1} stepped crystals between the sterile controls and G20 cultures at SI =

1.9 (sterile controls have ~ 14% fewer stepped crystals), and the dashed line shows where we would expect the same percentage in G20 cultures (corresponding to SI = 0.9).

Metabolic Uptake of Sulfate and Lactate as a Control on Calcite Morphology. The most commonly described mechanisms by which microbes stimulate calcium carbonate precipitation are the change of local pH (i.e., by photosynthetic uptake of carbon dioxide or by degradation of amino acids) and an increase in the amount of dissolved carbonate ions. However, in the well-buffered cultures of actively metabolizing G20, pH did not increase and DIC increased by only 2 ± 1 meq/L (measured in the absence of calcium) in the background of carbonate alkalinity of ~ 80 meq/L, as could be predicted for G20 cultures limited by 1 mM available sulfate. Consequently, G20 could not increase the SI by more than 0.1 SI units (modeled by MINEQL+ using the parameters in Table 1 and changing the total DIC by 2 mM, total sulfate by 1 mM, and total lactate by 2 mM). A much larger increase in SI (about 1 unit) is required to increase the percentage of {04.1} crystals by 14% (Fig. 3), implying that the metabolically induced increase of the alkalinity and the pH could not account for the observed differences in the shape of calcite crystals between G20 cultures and sterile controls. We therefore decided to test whether calcite morphology in the culture medium would change depending on the presence or absence of sulfate and lactate, substrates that are removed in active cultures of G20, but whose concentrations remain constant in sterile controls.

The presence of 2 mM sulfate in the medium without bacteria at SI = 1.2 increased the percentage of anhedral aggregates of bladed calcite (Fig. 2A - D) by about 50% relative to the medium without sulfate (two independent experiments). The addition of 3 mM lactate to the basal medium (SI = 1.5) without bacteria reduced the number of

truncated rhombohedral aggregates with stepped {04.1} faces and spars (Fig. 2H, J) by about 10% each, and increased the number of aggregates twinned on {01.2} and {10.4} (Fig. 2F, G) by about 20% (two independent experiments). The presence of 2 mM sulfate and 5 mM lactate in the medium reduced the crystallinity of calcite by 0.03 ± 0.01 °2θ. Lower crystallinity of the crystals grown with sulfate and lactate indicates either the presence of smaller crystallites or the presence of more crystal defects in the XRD sample. Even higher amounts of sulfate and lactate that are used in standard media for sulfate reducers (20 mM and 10 mM, respectively) reduced the total number of calcite crystals by as much as 50% (two independent experiments) and stimulated the growth of only hemispherical precipitates (Fig. 2A, D). The growth of calcite in the presence of sulfate and lactate at a given pH therefore resembled the growth of calcite in the absence of these ions, but at a lower initial pH.

Negatively charged ions like sulfate and lactate can affect calcite morphology by lowering the SI as they complex calcium ions and lower the pool of free calcium ions available for calcite precipitation [37]. Alternatively, they can be incorporated into the crystal lattice of growing calcite crystals, kinetically inhibit crystal nucleation, the growth of specific faces [61], or increase the number of defects in the crystal lattice. To distinguish between complexation and kinetic inhibition, we modeled the concentration of free calcium ions after complexation by sulfate and lactate in our medium by MINEQL+ (assuming the medium composition as described in Table 1 and varying the amount of Na-sulfate and Na-lactate). According to the model, the addition of 3 mM Na-lactate or 2 mM Na-sulfate would reduce the available calcium in the basal medium by less than 0.3 mM. Because we had to decrease the initial concentration of calcium in our

actual solution by much more (4 mM) to reproduce the same morphological changes, we conclude that complexation of the calcium ion by 3 mM lactate or by 2 mM sulfate cannot fully account for the observed changes in the calcite crystal habit. More likely, sulfate and lactate in G20 growth medium inhibit calcite growth kinetically. The observed changes of calcite morphology in active G20 cultures are thus consistent with the uptake of sulfate and lactate as kinetic inhibitors.

Hemispherical Crystal Habits Stabilized by Organic Compounds at Low SI. The prevalence of anhedral, hemispherical crystal habits at the lowest SI (Fig. 2A-D) contrasts with many reports of calcite precipitation in inorganic solutions that find or predict spars at low SI, and curved faces and spherical habits at high SI [35, 36, 62]. We hypothesized that the hemispherical habits at low SI developed under the influence of organic additives (0.05% by weight) in the basal medium. Indeed, when all the organic compounds were omitted from the basal medium (see Methods section), we did not observe hemispherical aggregates of bladed calcite (Fig. 4A-D). While inorganically precipitated calcite at high SI formed rounded aggregates (at $50\text{-}1\mu m$ scale), the crystallites that formed them were recognizably rhombohedral (Fig. 4C, D). Relatively low amounts (0.05 wt%) of organic compounds in solution can thus stabilize crystal habits that would not be expected in the absence of organics.
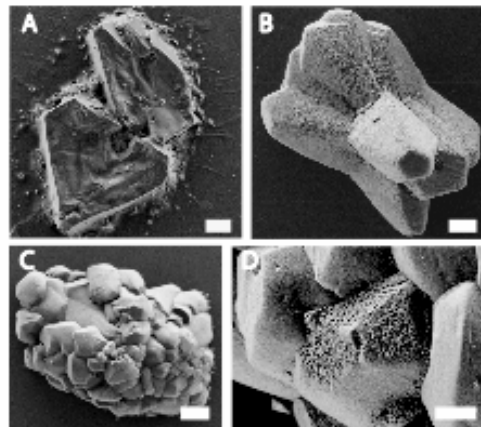
Figure 3-4   SEMs of calcite crystals precipitated in the presence and absence of organics in the basal medium. A) Inorganically precipitated calcite crystal at low SI in the absence of organic molecules. The scale bar is 10 μm. B) Rhombohedral calcite twin precipitated in the absence of organic additives in the basal medium at intermediate SI. The scale bar is 20 μm. C) Framboidal calcite aggregate precipitated at high SI. The scale bar is 20 μm. D) Rhombohedral calcite crystals within the aggregate from C). The scale bar is 5 μm.

Other studies have reported the formation of hemispherical and spherical calcite crystals in the presence of organic molecules and microbes [41, 43, 63]. Most of these studies found that calcite rhombohedra precipitated in their abiotic control solutions containing only inorganic calcium and carbonate salts (e.g., $CaCl_2$ and Na_2CO_3). Our inorganic control medium is a more realistic simulation of natural conditions because it contains magnesium, phosphate, sulfate, and trace metals that coexist in many natural waters, and are necessary for microbial growth. Although many of these inorganic ions are known to influence the growth and morphology of calcite [36, 39, 40, 64, 65], we did not monitor their concentrations in G20 basal medium after the precipitation experiment (Table 1). Therefore, we cannot discount the possibility that the uptake of trace amounts of inorganic inhibitors (e.g., phosphate) [40] may additionally contribute to the observed differences in calcite morphology between active cultures and controls (Fig. 1).

Our study supports the results of Braisant, Cailleau et al. [43] who found that the presence of less than 0.1% organic compounds in solution lead to the formation of spherical calcite habits. At a higher initial SI in G20 basal medium with the same organic

content, the organic influence diminishes, and these habits (Fig. 2A-D) are replaced by rhombohedral calcite habits that are less suggestively biogenic (Fig. 2E-L, Fig. 4A-D). Abundant calcite spheres and dumbbells in natural environments may therefore indicate conditions of relatively low SI in the presence of organic compounds (e.g., EPS or lactate).

However, calcite spherules and other anhedral precipitates may also form under abiotic conditions. Fernández-Díaz et al. [36] described an abiotic crystallization series of calcium carbonate in a gel and found Mg-calcite spheroids, dumbbells, and other anhedral precipitates at extremely high SI (~ 10 times higher than the highest SI in our medium). Tracy et al. (1998) reported the formation of spherulites in solutions that contained high concentrations of both magnesium and sulfate. The distinction between biogenic and abiotic spherulites may be possible if the abiotic ones form only in the presence of high sulfate and/or magnesium, and incorporate more magnesium or sulfate than the spherulites within biofilms. A comparative study of the bulk content and the zoning of trace sulfate, magnesium, and organic compounds in inorganically and biologically formed spherulites could help determine whether similar natural precipitates are biogenic or not. Biologically influenced end members could be distinguishable from the abiotic precipitates if they contain very low amounts of Mg and SO_4.

Effects of G20 Cellular Fractions and Biofilms on Calcite Morphology

Calcite crystals grown in the presence of G20 had more rounded edges than their counterparts in the sterile controls or UV-inhibited cultures (Fig. 1A-C). Because none of the previously examined parameters (SI, sulfate, lactate) could fully account for this

observation, it seemed likely that some kinetic inhibitors associated with metabolically active G20 cells and biofilms could explain this observation. In pursuit of these inhibitors, we compared the potential effects of specific compounds and cellular fractions of G20 that are in contact with the growing crystals in active cultures. G20 colonizes the growing calcite crystals (Fig. 5A) and secretes exopolymeric substances (EPS) (Fig. 5B) that are a complex mixture of proteins, nucleic acids, uronic acids, and other polysaccharides (e.g., Beech, Gaylarde et al. 1991). The outer part of G20's outer membrane (G20 is a Gram-negative bacterium) contains lypopolysaccharide (LPS) [66]. Lypopolysachharide consists of a hydrophobic lipid A, the core polysaccharide, and the O-antigen. The latter two components are rich in carboxyl and phosphoryl residues [66].
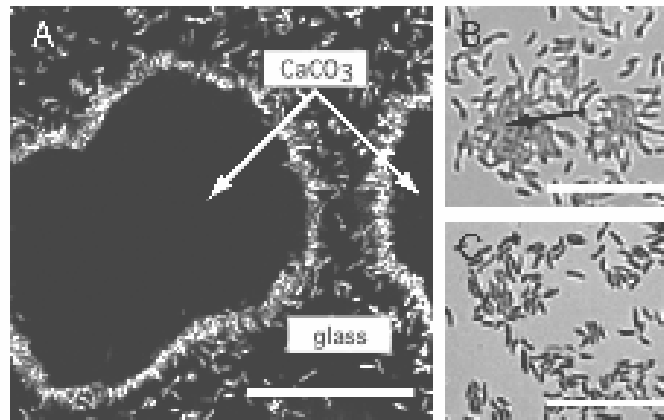
Figure 3-5   G20 forms thin biofilms and secretes exopolymeric substances (EPS) in calcite-precipitating cultures.   A) Confocal micrograph showing the attachment of fluorescently stained G20 to calcite crystals (dark dumbbell shapes marked by white arrows). G20 prefers the calcite crystals to the surrounding glass surface. The scale bar is 20 μm.   B) EPS (carbohydrates) were detected only in the centers of denser

microcolonies. EPS is the dark gray substance (black arrow). C) Duplicate controls slide with G20 biofilms grown and stained with a general bacterial stain as in Part B. EPS on this slide were not precipitated before staining. The scale bar in Parts B and C is 10 μm.

Both purified LPS and EPS rounded the edges of calcite crystals *in vitro* (Fig. 6), when added to the solution at a mass concentration that was approximately two orders of magnitude greater than in G20 cultures. We did not observe a similar effect in the presence of the outer membranes (not shown). The crystallites formed in the presence of EPS and LPS were also smaller and more numerous than the ones in control solutions without EPS and LPS added (Fig. 6), suggesting a role for these compounds in the nucleation of calcite (Bosak and Newman 2003).
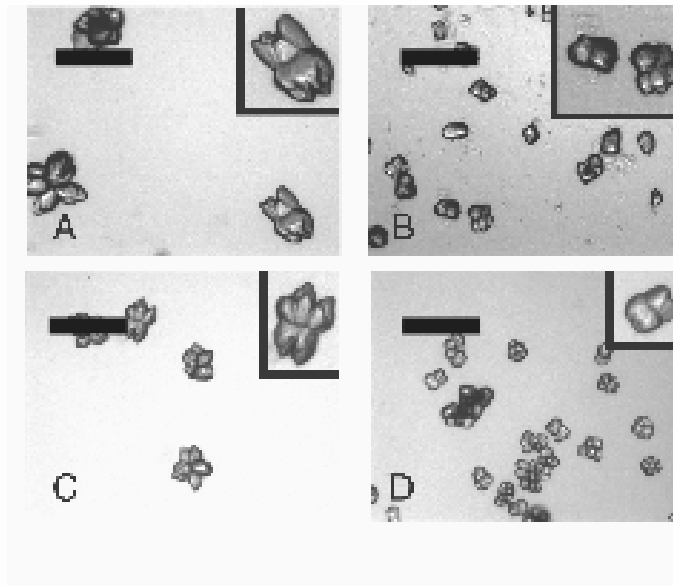
Figure 3-6 EPS and LPS of G20 can change calcite morphology. A) A typical field of view from the control medium without lypopolysaccharide (LPS) in a precipitation

experiment concurrent with Part B. B) A typical field of view in the presence of G20 LPS. The crystals are more rounded, less visibly striated, more numerous and smaller relative to Part A. C) A typical field of view from the control medium without exopolymeric substances (EPS) in a precipitate experiment concurrent with Part D. D) A representative field of view in the presence of G20 EPS (0.125 mg dry EPS/ml medium). As in Part B, EPS stimulated the growth of rounded crystals that were less elongated along the *c* axis, more numerous and smaller relative to Part C. The scale bar in all images is 200 µm.

     The difference in bacterial attachment and the secretion of EPS between live and UV-inhibited cultures may provide a clue about the differences between the calcite shapes in these cultures. Active G20 can attach to the growing mineral surface and locally expose crystals to high concentrations of LPS (Fig. 5A). In contrast, dead G20 and purified outer membranes sediment at the bottom of the culture wells to an average height less than 3 µm and can stick only to the lowermost surface of the growing calcite crystals (> 10 µm high). Moreover, given that we washed both the uninhibited and the UV-inhibited cells before the precipitation experiment to remove EPS, rounded crystal edges in metabolically active cultures appear to result mainly from the secretion of new EPS (Fig. 5B). Similarly low amount of organics can be expected to affect calcite morphology in natural microbial biofilms. Namely, the secretion of small amounts of kinetic inhibitors (e.g., EPS, LPS) very close to the growing crystal could suffice to change the crystal habit, even when the concentrations of dissolved organics in the bulk solution is low.

Rounding of calcite edges due to the development of high-index faces has been observed in some studies of the effects of carboxylic acids, amino acids, and proteins on calcite morphology [42, 63, 67, 68]. Chemical analysis (two independent experiments) showed that EPS from G20 cultures contained 3 ± 1 µg/mg EPS more protein than the background sterile medium. Qualitative gel assay confirmed that EPS from G20 cultures also contained more nucleic acids (data not shown), 0.10 ± 0.01 µg/mg EPS more uronic acids, and 9 ± 6 µg/mg EPS less carbohydrates than the background medium. These chemical differences are consistent with the hypothesis that negatively charged moieties of G20 EPS (as found in protein, DNA, RNA, and uronic acids) bind calcium or even incorporate into the growing crystals, inhibiting the growth or twinning along some crystal plains. A higher carbohydrate content (neutral sugars) in the sterile medium may be due to the unmetabolized components of the yeast extract and suggests that the net observed differences between active cultures and controls may be partially due to the metabolic alteration of complex organic additives (yeast extract and vitamins) by G20. Unfortunately, rounded edges and curved surfaces of rhombohedral calcite alone are not a good biomarker, inasmuch as similar features have been reported in presumably inorganic solutions at extreme supersaturation values [35].

Conclusions

In summary, calcite crystals that precipitated in metabolically active cultures of *D. desulfuricans* G20 were morphologically distinct from the precipitates in sterile controls and UV-inhibited cultures. Biological mechanisms that provide consistent explanations of these differences are: microbial removal of kinetically inhibiting

metabolites (sulfate, lactate and, likely, minor inorganic and organic nutrients), the concurrent secretion of EPS, and the interactions between the growing crystals and the LPS of actively colonizing bacteria. On the other hand, both our calculations and our measurements show that microbially induced shifts in the SI were much less important, because the medium is well buffered by high DIC. This is consistent with the model of Arp et al. (2001) where calcification within biofilms in the presence of comparably high DIC occurs within the EPS, instead of being induced by photosynthetic changes of SI on the sheaths of photosynthetic bacteria. Because calcification within biofilms can be kinetically stimulated or inhibited relative to the outside environment at the microscale, it is important that the search for robust morphological indicators of bacterial presence be performed at this scale [11].

Overall, although we could expect rapid nucleation of many small crystal grains (whitings), due to the high SI of our medium, we found that fewer large crystals grew instead. This appears to be caused by the presence of many kinetic inhibitors in the solution. Our results show that microbes can exert kinetic control not only by the secretion of exopolymeric substances [32, 43] but also by the active uptake (or release) of primary organic and inorganic metabolites. Extending these observations to the field, we infer that microbial production or removal of kinetic inhibitors may have controlled calcification within biofilms in highly supersaturated environments, both ancient (Precambrian oceans) and modern (soda lakes and travertine deposits).

4. A laboratory model of abiotic peloid formation

Abstract

Peloids are rounded grains of micritic calcite whose origin has been attributed to various biological and abiotic mechanisms. To constrain abiotic parameters that favor the formation of peloids, we precipitated calcite crusts in the absence of microorganisms. Clotted opaque fabrics that formed during the initial stages of the experiment consisted of ~10 μm peloids, while compact clear sparitic crusts precipitated in subsequent stages. The increasing supersaturation of the solution in time is responsible for this morphological succession. Initially, peloids form by the radial growth of spar crystals around a small number of nuclei. As the supersaturation increases, more spar crystals nucleate and aggregate non-radially into compact crusts. Rounded clotted precipitates are a consequence of the growth in suspension and geopetal settling, and isopachous crusts grow in the absence of these processes. Although peloids are commonly assumed to have a microbial origin, our results show that very similar morphologies can be created by purely abiotic mechanisms. Thus, the biological origin of rounded micritic calcite grains in the rock record must be verified against the abiotic null-hypothesis in each specific case.

Introduction

A good biomarker is a crystal and rock morphology is difficult or impossible to produce abiotically. It is thus particularly challenging to recognize morphological

biosignatures in common sedimentary carbonates (e.g., calcite or aragonite) because the morphology of these minerals can be controlled by a daunting number of inorganic and microbial processes. Peloids, defined as 10-60 m in diameter "more or less rounded grains of homogeneous micrite" [69], are an example of calcite grains whose origin has been explained by a diversity of biotic and abiotic hypotheses.

Peloids are a ubiquitous facies in both modern and ancient carbonate rocks. They can be found in open marine spaces, encrusting sponges [70], forming laterally extensive layers in Triassic, Jurassic and Permian reefs [71-74], mud mounds [75], fast-precipitating Neoproterozoic deposits (A. Maloof, personal communication) and Proterozoic stromatolites [76, 77]. However, peloids are often confined to more restricted spaces such as skeletal cavities in marine environments [71, 72, 78, 79]. Peloids can also be found in terrestrial environments like caves [80] and travertines [81].

Sundry abiotic processes can contribute to the creation of rounded carbonate grains in these diverse chemical, ecological and physical settings. Peloids have been interpreted as detrital grains [82], an intermediate stage of development of microcrystalline calcite cement [83] or as the product of repeated nucleation of dentate rims around submicrocrystalline centers of growth [84]. Arguments in favor of a biogenic origin of peloids are based on the occasional association of peloids, spherulites and peloidal crusts with organic matter or putative microbial remnants [70, 74, 81, 85, 86]. Some biological mechanisms that have been used to explain the origin of rounded calcite grains are: the calcification of algal filaments and coralline algae, fecal pellets (see Ref. [79] for a discussion of these mechanisms), the stimulation of calcium carbonate

nucleation within acidic mucoproteins [86] or around unspecified bacterial clumps [81, 87, 88], and nucleation around cyanobacterial cells [74, 85, 89].

The goal of this study was to test whether purely abiotic processes can lead to the formation of a morphologically distinct type of marine peloids: one containing a submicrocrystalline center commonly surrounded by a well-developed euhedral rim of sparry, dentate calcite [79]. Extending our previous studies of the microbial influence on the nucleation and morphology of calcite from single crystals in batch culture to calcite crusts in continuous culture, we found clotted layers composed of peloidal grains in the crusts [8, 9]. Here, we relate these abiotically precipitated fabrics to the chemical and physical parameters in our solutions and discuss what these laboratory results imply for the recognition of similar precipitates in the rock record.

Materials and methods

Precipitation reactor. To maintain a constant supply of calcium and bicarbonate ions, calcite crusts were grown at 25°C and at pH 7.5 (checked by pH paper) in a medium described by Bosak & Newman [8] in a 420 ml working volume disk reactor (Biosurface Technologies Corp.). The reactor was regularly checked for contaminants both visually (by monitoring the turbidity or fluorescently staining and imaging the outflow) and by plating the outflow. Two fresh sterile media were added in equal proportions to the reactor through air-tight Tygon® tubing: one from a sterile reservoir containing 40 mM $CaCl_2$ (pH 7.2, 1 atm N_2 gas phase), the other from a sterile reservoir containing 140 mM $NaHCO_3$ (pH 8.2, 0.15 atm CO_2 and 0.85 atm N_2 gas phase). A peristaltic pump regulated the rate of inflow (~80 ml/hr of the combined medium through the reactor).

The medium was stirred by a magnetic stir bar. The headspaces of the reservoirs and the flow-through reactor were flushed with a 0.85 atm: 0.15 atm N_2/CO_2 gas mix (mixed by a FM-1050 Matheson Tri-Gas[®] flowmeter). A maximum of twenty-four 1-cm diameter polycarbonate and glass chips provided removable surfaces for the growth of the crusts. The chips were taken out from the reactor daily over the course of four days.

Aragonite precipitates. Aragonite seeds were precipitated under sterile conditions in the modified ATCC2056 seawater (SW) medium that contained 10 mM $CaCl_2$ (final concentration in the reactor), 50 mM $MgCl_2$ and 400 mM NaCl, 125 ml/l of marine seawater mix (7 g/l $MgSO_4$ x $7H_2O$, 3.24 g/l Na_2SO_4, 1.2 g/l KCl, 0.1 g/l Na_2CO_3, 0.1 g/l NaBr, 80 mg/l KBr, 72 mg/l $SrCl_2$ x $6H_2O$, 52 mg/l H_3BO_3, 8.1 mg/l Na_2HPO_4, 2.4 mg/l NaF, 0.4 mg/l Na-silicate, 50 g/l KI) and 10 ml/l SL-10B trace metal solution. Crystals were collected in a sterile fashion after 12 hours of continuous precipitation, pulverized mechanically, and used as nuclei for the subsequent precipitation experiment in the SW medium at different initial pH (7.2, 7.5, 7.8 and 8.0). The nuclei were incubated in sterile SW medium in 8-well LabTek[®] (NalgeNunc International) culture dishes with coverslip bottom in the anaerobic chamber (0.15 atm CO_2, 0.05 atm H_2 and 0.80 atm N_2) for 8 days.

Imaging

SEM imaging. Chips with calcite crusts were fixed in Karnovsky fixative [90] after collection and then rinsed three times in cacodylate buffer (0.2 M, pH 7.5). The samples were postfixed with 1% OsO_4 in water for 5 hours followed by several rinses in cacodylate buffer, dehydrated in a graded series of ethanol (30, 50, 70, 90 and 100%) and

progressively infiltrated with LR-White resin for six hour prior to polymerization at 65°C for 24h. After the polymerization, a transverse section of the crust was polished [91] and carbon coated. The samples were viewed either on an XL 30 ESEM-FEG Philips scanning electron microscope (SEM) operating in high vacuum using the backscattered electron detection imaging system at 15 kV and a working distance of 10 mm, or on a LEO 1550 VP SEM operating at 15 kV and a working distance of 10 mm. The elemental composition was determined by EDS using a LEO 1550 VP SEM operating at 15 kV and at a working distance of 13 mm. Aragonite clots were imaged unembedded and unpolished.

Transmitted light microscopy. Images of 30 μm thin sections of the calcite crusts were taken with a Zeiss Axioplan microscope. Aragonite peloids were imaged through the coverslip bottom of the culture dishes by an inverted Zeiss Axiovert S100 microscope.

Mineral analysis. The crystal structure of the precipitates from the reactor experiments (calcite and aragonite) was determined by X-ray diffraction using a Scintag diffractometer at Cu Kα (λ=1.5405 Å). The crystals were washed with 10% bleach and rinsed in doubly distilled water before analysis. When only little sample could be retrieved (from LabTek[®] NalgeNunc International culture dishes with aragonite nuclei), we could not obtain the X-ray diffraction spectrum. Instead, we analyzed these precipitates by Fourier transform infrared spectrometry (FTIR) on a SensIR Technologies DuraScope[TM]. Aragonite was distinguished from calcite by its peak at 1082 cm^{-1} and the peak at 852 cm^{-1} [92].

Results

Rounded peloidal precipitates similar to those described by Aissaoui [93] formed in the initial, clotted stage of abiotic calcite crust precipitation.   Later precipitates consisted of dentate spar crystals that aggregated into compact crusts (Fig. 1A, B).   The peloids were round, 10   m ± 3   m in diameter (N=87).   Their submicrocrystalline centers consisted of radially growing acicular crystals less than 1   m thick. Microcrystalline rims of dentate spar crystals grew radially around the centers (Fig. 1C, D).   The centers appeared dark under the backscattered SEM, suggesting a higher abundance of lighter elements relative to the rims (Fig. 1D).   Indeed, EDS analysis showed that the P content was higher in the centers (0.69 ± 0.36 wt%, N=13) than the rims (0.12 ± 0.09 wt%, N=13) and later stage compact crusts (P below detection limit). The opaque appearance of peloids under the transmitted light (Fig. 1E, F) was mainly a consequence of the small crystal grain size relative to the thickness of the thin-section (30 μm).   The later compact crusts of large dentate spar crystals were clear under the transmitted light (Fig. 1B, E, F).
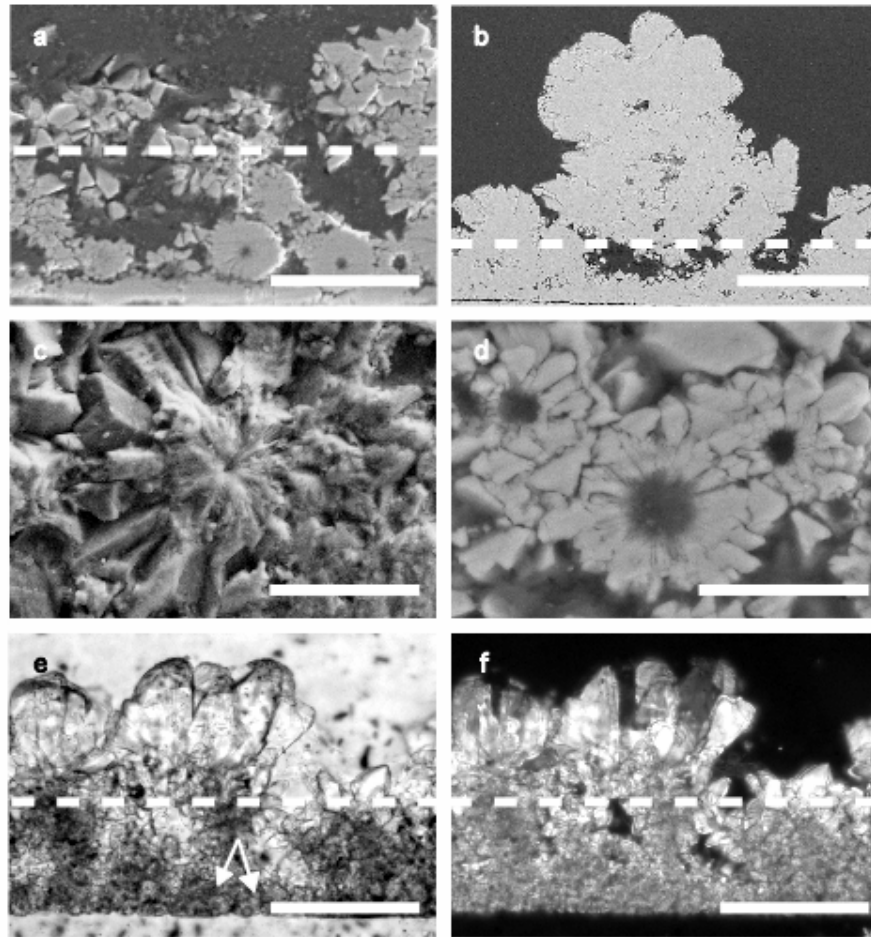
Figure 4-1   Experimentally precipitated calcite crusts in the absence of bacteria. A. A

backscattered SEM of one-day-old crusts with peloids on the bottom and the later non-

radial crystal aggregates (above the dashed line). The dark area is resin. The scale bar is

20 μm. B. A backscattered SEM of four-day-old crusts with the peloid layer on the

bottom and the later compact crusts (above the dashed line). The dark area is resin. The

scale bar is 100 μm. C. A SEM showing the internal fabrics of an unpolished peloid: a

round core composed of thin radially arranged crystals and a rim made of coarser dentate

spar crystals. The scale bar is 10 μm. D. A backscattered SEM of peloids shows the

radial arrangement of the spar crystals around a common center. The scale bar is 5 μm.

E. Opaque layer of peloids (below the dashed line) rimmed by large later crystals (transmitted-light image of a thin section of the four-day old crust). Individual peloids can be seen at the bottom of the section (arrows). The scale bar is 50 μm. F. Polarized-light image of the same field of view as in E. The scale bar is 50 μm.

Supersaturation

Given that peloids in our experiments precipitated in the absence of bacteria, we sought to determine which abiotic mechanisms were responsible for the precipitation of rounded centers of peloids, spar rims, and the later large spar crystals. Many studies of calcite morphology in abiotic solutions [34, 36, 94] report that the calcite saturation index (SI) exerts a major control over calcite morphology. The SI of calcite (or aragonite) in a solution depends logarithmically on the calcium ion concentration, $[Ca^{2+}]$, the carbonate ion concentration, $[CO_3^{2-}]$ and the solubility constant of calcite (aragonite), K_s:

$$SI = \log \frac{[Ca^{2+}][CO_3^{2-}]}{K_s} \qquad (1)$$

Consistent with the previous studies, the changes in SI in our precipitation medium result in a predictable trend of calcite morphologies when tested in the absence of flow (batch conditions) [9]. Furthermore, the habits developed in the batch SI sequence have their counterparts in the habits of calcite crystals that grew in the continuous-flow reactors

(Fig. 2A). Namely, the cores of peloids (Fig. 1C) are similar to the hemispherical crystals composed of bladed crystallites that form at the lowest SI under batch conditions (0.5 ≤ SI ≤ 1) (Fig. 2A). Peloidal rims (Fig. 1C) are, in turn, similar to the radially aggregating spar crystals that grow at a relatively low SI (1 ≤ SI ≤ 1.5) in the absence of flow (Fig. 2A). The non-radial aggregates of spar crystals in the clear crusts resemble spar crystals observed at even higher SI in the batch experiments (1.5 ≤ SI ≤ 2.0) (Fig. 2A).

Given that the concentration of calcium in the reactor gradually increases in the beginning of the experiment (see Methods), the observed morphological trends in calcite crusts can similarly be attributed to the increasing SI in the flow-reactor. The temporal change in the calcium concentration in the reactor can be described by

$$\frac{d[Ca^{2+}]_{reactor}}{dt} = \frac{f([Ca^{2+}]_{in} - [Ca^{2+}_{out}])}{V_{reactor}} - R \tag{2}$$

where f is the flow rate, $[Ca^{2+}]$ is the calcium concentration, t is the time, V is the volume of the reactor (420 ml), and R is the rate at which $CaCO_3$ precipitates in the reactor. Because $[Ca^{2+}]_{out}$ is equal to $[Ca^{2+}]_{reactor}$, solving the equation (1) for $[Ca^{2+}]_{reactor}$ gives

$$[Ca^{2+}]_{reactor}(t) = ([Ca^{2+}]_{in} - \frac{V_{reactor}R}{f})(1 - \exp(-\frac{ft}{V_{reactor}})) \tag{3}$$

When the flow starts, the calcium concentration in the reactor increases (Fig. 2B) to an equilibrium value that depends on the precipitation rate, the flow rate, the dimensions of

the reactor and the rate of supply of the calcium ions (Fig. 2B and Eq. 3). The modeled increase in SI is consistent with the appearance of various crystal habits in the crusts over time. The spherical aggregates of submicrocrystalline calcite that form the cores of peloids precipitate at the lowest SI (and calcium concentrations below about 10 mM). Small dentate spar crystals, such as those found at the rims of the earliest, smallest peloids, do not precipitate in batch experiments unless at least 10 mM $[Ca^{2+}]$ is present. More than 15 mM $[Ca^{2+}]$ is required for the precipitation of larger spar crystals (as found in the rims of later peloids) and non-radial spar aggregates. Equation 3 predicts that 10-15 mM $[Ca^{2+}]$ in the reactor would be reached in about 10-15 hours (assuming that calcium ions are removed from the reactor by the precipitation of calcite at a uniform rate from 0 mM/hr to 1 mM/hr, Fig. 2B). When $[Ca^{2+}]$ in the reactor exceeds this limit, non-radial spar aggregates can precipitate; they form the upper part of 1-day old crusts and all subsequent precipitates. This model prediction is consistent with our experimental observations: peloids are present only in the lower half of our 1-day precipitates and do not occur in the later (upper) stages (Fig. 1A, 1B).
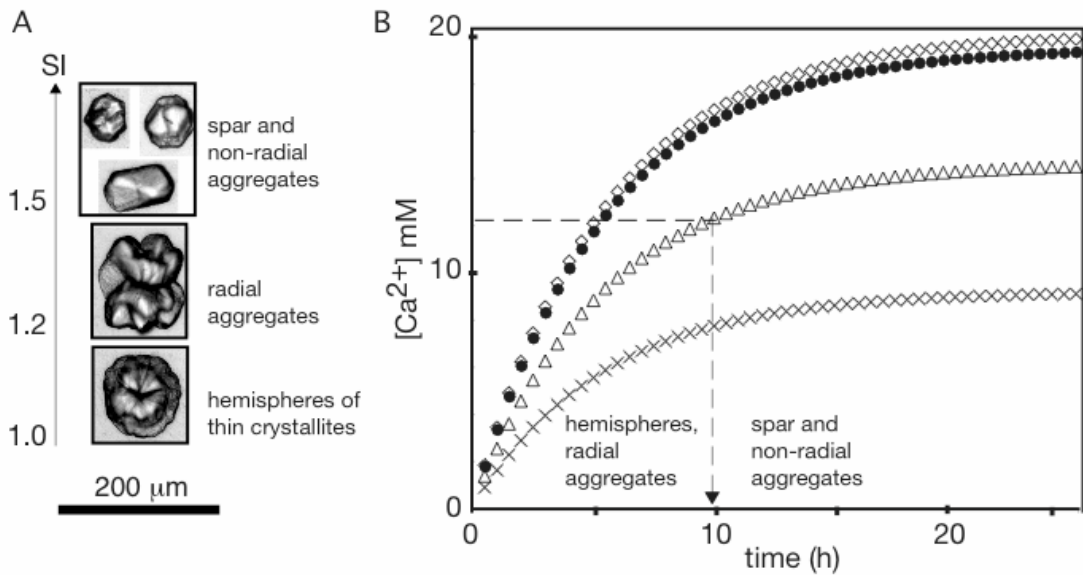
Figure 4-2   A. Representative calcite crystal morphologies as a function of the initial

supersaturation index (SI) in the batch precipitation experiments. The vertical arrow

indicates the increasing initial SI (established either by changing the pH, or the calcium

ion concentration). All crystals are shown to scale (indicated by the 200 μm scale bar).

B. Calcium concentration in the continuous-flow precipitation experiment as a function

of time based on Eq. 3 assuming four different precipitation rates within the reservoir (0

mM/hr: ◇, 0.1 mM/hr: ●, 1 mM/hr: △, 2 mM/hr: ✗). The dashed line shows the time

when the calcium concentration rises to values at which non-radially aggregating spar

crystals precipitate instead of radial aggregates.   This estimate assumes that the

precipitation rate is 1 mM/hr (△) and that the minimum calcium ion concentration

needed for the formation of large spar crystals and non-radial spar aggregates at pH 7.5 is

12 mM (as determined in the previous batch experiments). Slower precipitation rates

correspond to shorter times before non-peloidal precipitates are observed and faster

precipitation rates correspond to longer times than 10-15 hours, respectively.

To demonstrate that rounded calcium carbonate grains can form in solutions more analogous to seawater that have few or no organic additives such as yeast extract or lactate, we conducted a precipitation experiment in sterile artificial seawater medium without organic constituents. This time, opaque 46 μm ± 36 μm mean diameter (N=35) rounded clusters of acicular crystals aggregated into clotted crusts (Fig. 3A, B). XRD analysis confirmed that they consisted of aragonite. These clotted precipitates appear identical to the aragonite clots that grew in seawater in laboratory experiments described by Taylor & Illing [95]. Rounded aragonite grains are also common in reef settings and geochemically distinguishable from calcite peloids [79, 95]. To test whether their morphology also depends on SI, we used small (< 20 m) aragonite grains as the nuclei for further crystal growth in the seawater medium at different initial SI under batch conditions. Large transparent rims surrounded the opaque aragonite seeds at initial pH 7.2-7.5 (Fig. 3C). An increased SI facilitated the nucleation of many shorter acicular crystals that encrusted the seeds in a less orderly manner, creating the opaque rounded and clotted aggregates at initial pH 7.8-8.0 (Fig. 3D). Additionally, the absence of nuclei in the same solution resulted in very few (~20 per entire well) clear rounded grains without opaque centers at low initial pH (not shown) and clear subhedral grains (about 10 in the same field of view as in Fig. 3C or 3D) at high initial pH. Similar subhedral clear grains were abundant at high initial pH even in the presence of seed crystals (Fig. 3D).
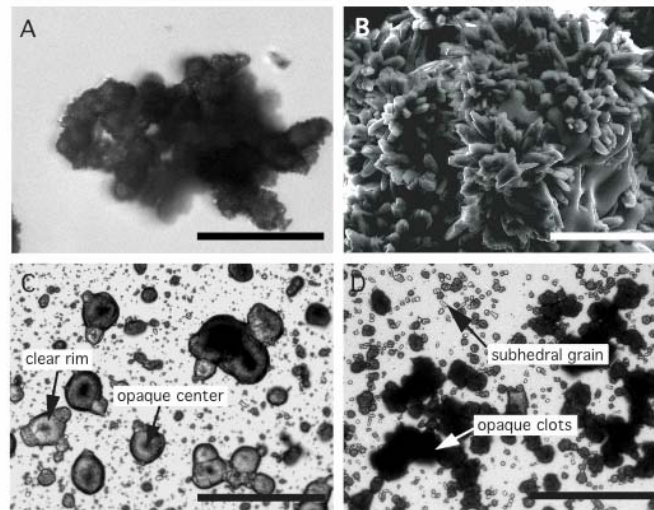
Figure 4-3   Aragonite precipitates and their fabrics as a function of the initial pH. A. A rounded opaque cluster of acicular aragonite crystals (transmitted light, a larger than average aggregate is shown to illustrate the clotted fabrics). The scale bar is 50 μm. B. Aragonite needles that constitute the opaque aggregates (SEM image). The scale bar is 2 μm. C. Transparent aragonite rims around the opaque aragonite seeds at pH 7.2 under transmitted light. The scale bar is 200 μm. D. Opaque clotted aggregates precipitated around the opaque aragonite seeds at pH 8.0. Subhedral spar crystals are also present. The scale bar is 200 μm.

Stirring and Settling

Peloids that grow suspended in the stirred reactor are spherical, whereas the grains grown under batch conditions (i.e., not suspended) are hemispherical, with a flat bottom due to growth on a flat glass slide (Fig. 2A, 4A).

Settling also has a role in creating morphological differences between the downward-growing calcite crusts on the bottom surfaces of the chips and the upward-growing peloidal crusts on the top surfaces of the chips. In contrast to the clotted fabrics of the upward-growing crusts, the downward-growing crusts were clear, uniformly thick (isopachous) aggregates of spar crystals (Fig. 4B, C). Thus, geopetal settling and rapid *in situ* cementation produce clotted and non-isopachous fabrics, while only the latter mechanism is responsible for the isopachous compact crusts on the vertical and the bottom sides of the chips.
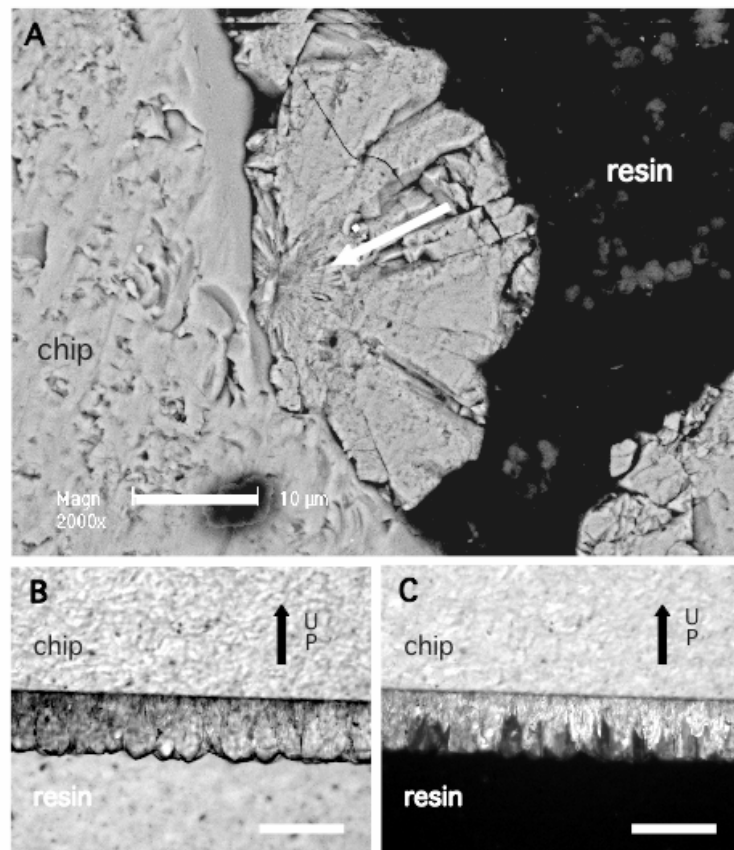
Figure 4-4   The importance of stirring and gravitational settling for the formation of spherical habits. A. A backscattered scanning electron micrograph of a hemispherical

calcite crystal precipitated in G20 growth medium in a batch experiment (as opposed to the crusts formed in flow-through reactors). The arrow points to the submicrocrystalline core. The scale bar is 10 μm. B. Four-day old isopachous calcite crusts on the bottom surface of the chips. The arrow marks the upward direction. The scale bar is 100 μm. C. Polarized-light image of the same field of view as in F.

Discussion

How to infer the extent of abiotic vs. biological contributions to the formation of calcium carbonate structures such as peloids at various times throughout Earth's history has been an open and intriguing question in sedimentary geology. At the heart of this problem lies the fact that microbes can stimulate all abiotic aspects of mineral nucleation and precipitation. Good abiotic models are therefore a prerequisite for the recognition of putative biological contributions to the generation of peloids and other carbonates. Towards this end we have generated calcite peloids in the complete absence of microbes and have developed an abiotic model that can explain their shape. In the following discussion, we relate this model to some natural physical, chemical and biological processes that generate calcium carbonates, and discuss the caveats it raises regarding the commonly assumed microbial role in peloid formation.

Stirring is a simple, but important physical process required for the formation of rounded peloids in our solutions. Our observations support Lighty [78], who attributed the spherical shape of peloids within coral skeletal cavities in a reef to the growth of peloids in prolonged suspension. Similarly, peloids have to remain suspended in solution

during the growth of spar rims if these uniform rims are to form by slow growth around the initial submicrocrystalline nuclei [84].

Chemically, the generation of rounded calcite grains in our medium was greatly influenced by SI. In nature, changes in the SI of calcite can occur by various mechanisms: mixing of waters rich in calcium with waters that contain a high concentration of dissolved inorganic carbon (DIC) [96], wave agitation [95], degassing of CO_2, evaporation, tidal forcing, flow through cavities in reefs, or changes in temperature. SI is not the only possible parameter that can affect peloid formation. Various kinetic inhibitors (e.g., magnesium, phosphate, sulfate) can additionally influence the morphology of calcite by incorporating into the growing crystal lattice and thermodynamically stabilizing various crystal faces, increasing the number of defects, or changing the solubility of the mineral [36, 38-40]. The addition or removal of various kinetic inhibitors may exert a greater control on calcite morphology than the changes of SI in solutions that are buffered by a high concentration of DIC [9]. Nevertheless, the SI controls the number of nuclei around which peloids can precipitate [8] and the shape of clotted precipitates (Fig. 2A, Fig. 3C,D).

Our medium was designed to mimic modern-day travertines, soda lakes and the Precambrian oceans rather than modern-day marine settings and therefore contains a high concentration of DIC. Its SI is much higher than that of the modern seawater, and is thus responsible for the easy nucleation and precipitation of calcite. Because an even greater abundance of nuclei (at higher, final SI in our medium) results in the formation of non-radially aggregating calcite crystals, we infer that both laboratory-made and natural calcite peloids reflect the limited availability of nuclei or templating surfaces. The

formation of a limited number of calcite nuclei and the subsequent precipitation of spar rims is consistent with the proposed mechanism of abiotic peloid formation by repeated nucleation [84]. The dentate rims of these peloids are attributed to the slow precipitation around the initial nuclei (possibly at a lower SI).

Facilitated nucleation and precipitation of calcite may similarly explain an increased abundance of peloids at various times of the Earth's history relative to the present time. Namely, while modern peloidal crusts are associated with mucoid surfaces and microcavities, some ancient peloidal layers occur in considerably more extensive settings and under a wider range of environmental conditions than today. For example, peloids were a common facies in carbonate reefs before the advent of skeletal organisms [76, 77] and Neoproterozoic cap carbonate deposits (A. Maloof, pers. communication). In addition, some peloids in end-Permian and Upper Jurassic reefs can be linked to the presence of coccoidal microbes (presumably cyanobacteria) [72, 74, 85, 89]. Because their modern marine encrusted cyanobacterial analogs are relatively rare, this suggests that these peloids formed under different environmental conditions [97]. A different seawater chemistry [89, 98, 99], removal of kinetic inhibitors [9] and/or increased temperatures [97] are just some of the potential explanations for the more widespread occurrence of peloids in the past.

Microbes can significantly stimulate abiotic nucleation and precipitation of carbonate minerals by inducing all of the chemical and physical conditions listed above: they can change the pH or the alkalinity of the solution, take up and secrete various kinetic inhibitors or bind calcium and magnesium ions on their negatively charged outer surfaces [8, 9, 14, 41-48]. Organic compounds with acidic moieties that are common in

biofilms can also stabilize different calcium-carbonate polymorphs [43, 100]. Additionally, the biofilm matrix can facilitate growth of spherical precipitates even when stirring is negligible by trapping the settling precipitates. As a result, many peloids have been spatially correlated with microbial biofilms [89], organic matrices [86], or single cells [74].

Arguments for a microbial role in the precipitation of some marine peloids and peloids in modern travertines are typically based on the following observations: the opaque appearance of travertine peloids under transmitted light, the occasional presence of micropores in the centers of travertine peloids, and the presence of putative microbial remains in the centers of marine peloids [81]. Our experiments show that peloids and other rounded grains with opaque centers can form in the complete absence of microbes (Fig. 1, Fig. 3C) and that microbes can become entombed in calcite even when they do not significantly stimulate its nucleation, leaving abundant micropores [11]. Moreover, microbes and their biopolymers have been reported to stimulate the dissolution [101] or inhibit the precipitation of calcium carbonate [32]. Therefore, independent experiments are required to confirm whether microbes contributed to the precipitation of peloids or merely colonized them. For example, elemental and isotopic differences between peloids and adjacent cements or a consistent association of fossilized cells with the centers of peloids might be persuasive evidence in favor of a microbial role in peloid formation. If such data are not available, our results suggest that abiotic mechanisms should be the null-hypothesis.

Conclusions

Our studies demonstrate that peloids can be created by purely abiotic mechanisms, suggesting that similar processes are likely to be important in nature. The internal fabrics of individual peloids (submicrocrystalline centers and dentate spar rims) can be explained by the changes in the calcite SI in the fluids from which peloids precipitate. Radiating crystal rims around submicrocrystalline nuclei imply that the number of nuclei controls peloid formation because random, non-radial sparitic aggregates form when nucleation is not inhibited. Microbial processes have the potential to stimulate or inhibit all stages of peloid formation. Therefore, microbial colonization of peloids in most cases cannot be used to infer a biological origin of these grains. Because multiple mechanisms can be simultaneously involved in the formation of similar fabrics, peloids are a poor indicator of environmental conditions and biological processes.

5. Micrometer-scale porosity as a biosignature in carbonate crusts

Abstract

We formed calcite crusts in the presence and absence of the heterotrophic bacterium *Desulfovibrio desulfuricans* strain G20 to investigate microbial morphological signatures in fast-accreting carbonate precipitates. Submicrometer- to micrometer-sized pores (micropores) were present and ubiquitous in the G20 crusts but absent in abiotically precipitated crusts. Bacterial micropores resemble inclusions under transmitted light but have distinct size, biological shapes and patterns (swirling or dendritic), and are distributed differently from common fluid inclusions. We observed similar porosity in both modern and ancient carbonate crusts of putative biotic origin. Our experiments support the microbial origin of micropores and help define specific criteria whereby to recognize these features as biosignatures in the rock record.

Introduction

Microfossil-like structures of uncertain origin (e.g., putative Archean microfossils, "nanobacteria" in terrestrial and meteoritic samples) often provoke intense scientific debate because of their potential implications for the evolution of both terrestrial and extraterrestrial life [33, 102-104]. It is therefore important to resolve how and why such structures form, whether they are biogenic at all, and whether similar structures can form abiotically.

Micropores (sensu Ref. [105]) constitute one such ambiguous biomarker. Micrometer-sized micropores have been most thoroughly described in the context of fast-accreting hot-spring travertines [105], but abundant pores whose sizes and shapes resemble microbial cells can be found in SEM (scanning electron microscopy) images from diverse environments such as beachrock and other modern and ancient marine cements [106, 107]. Evidence for the biological origin of micropores has so far been based on the comparison of their size and shape to both putative and well-preserved microorganisms found around dendritic micritic aggregates or "bacterial shrubs" in travertine hot springs [88, 105, 108, 109]. However, although a link between microbes and micropores has been suggested, it has not been experimentally demonstrated. Furthermore, even if *a priori* we were to accept micropores as a biomarker, it is important to understand what microbial processes and precipitation rates lead to their formation and how they can be distinguished from abiotically occurring porosity and/or fluid inclusions [110].

To help interpret micropores and experimentally develop criteria for the recognition of micropores as a biosignature, we precipitated carbonate crusts in the presence and absence of *Desulfovibrio desulfuricans* strain G20 in a medium highly supersaturated with respect to calcium carbonate [9]. We compared our laboratory findings to micropores in a modern and an ancient carbonate crust.

Materials and methods

Biofilm reactor. To maintain a constant supply of nutrients, calcium, and bicarbonate ions, G20 biofilms were grown at room temperature in a stirred-disk reactor

having a 250 mL working volume (Biosurface Technologies Corp.). Biofilms were established by growing G20 in the absence of calcium in a medium described by Bosak and Newman [8] for two days before the flow was started. An identical but uninoculated reactor was set up in parallel as a sterile control. The headspaces of the reservoirs and the biofilm reactors were flushed with an 85:15 N_2/CO_2 gas mix to keep them anaerobic. Twenty-four 1 cm diameter polycarbonate and glass disks provided removable surfaces for biofilm and crust samples. Three disks were taken out from both the sterile and the inoculated reactor daily over the course of four days. We performed two separate precipitation experiments to verify their reproducibility.

Backscattered SEM imaging. The disks with carbonate crusts were fixed in Karnovsky fixative after collection [90]. The remains of the fixative were removed with several rinses with cacodylate buffer (0.2 M, pH 7.5). The samples were postfixed with 1% OsO_4 in water for 6 h, rinsed several times in cacodylate buffer, dehydrated in a graded series of ethanol (30%, 50%, 70%, 90%, and 100%) and progressively infiltrated with LR-White resin for 6 h prior to polymerization at 65 °C for 24 h. After the polymerization, a transverse section of the crust was polished [91] and carbon coated. The samples were viewed on an XL 30 ESEM-FEG Philips operating in high vacuum using the backscattered-electron–detection imaging system at 15 kV at a working distance of 10 mm. The petrographic thin sections of natural samples (discussed below) were polished, carbon coated, and imaged by a LEO 1550 VP SEM equipped with an energy-dispersive X-ray spectrophotometer (EDS) using the backscattered-electron detector operating at 15 kV and a working distance of 10 mm. We measured the amount of precipitate on the chips (approximated by the surface area covered by the crusts in 10

successive SEM images of a random vertical cross section of the samples) by MetaMorph imaging software. Although MetaMorph cannot measure the porosity of the samples directly, it easily distinguishes between calcite crusts and cavities or bacterial aggregates. Thus the apparent thickness measured by MetaMorph can be used as a proxy for the total amount of precipitate.

Epifluorescence and transmitted-light imaging. Fixed carbonate crusts precipitated in our laboratory experiments were cut by a sterile razor, stained by FM[®] 1-43 fluorescent membrane stain, and imaged by a Zeiss Axioplan microscope. Petrographic thin sections were examined with a Zeiss Axioplan polarizing microscope and imaged with a Zeiss MRm 12-bit digital imaging system.

Results

Microfabrics of Laboratory Precipitates in the Presence and Absence of Bacteria

Under our experimental conditions, calcite readily precipitates from the solution even in the absence of bacteria [8, 9]. Given that ~100 μm thick crusts accreted both in G20 and sterile reactors in 4 days, we found that the most obvious morphological difference between the biotic and the abiotic samples was the presence of abundant micropores in the G20 crusts (Fig. 1 and Fig. 2).

The porosity produced by biological mechanisms can be attributed to the presence of cells and easily distinguished from the abiotically formed porosity (Fig. 1). Submicrometer- to micrometer-sized micropores (width = 0.3 ± 0.1 μm, median = 0.3

µm, length $= 0.7 \pm 0.3$ µm, median $= 0.6$ µm, number $N = 114$) extend three-dimensionally from the dense G20 cell aggregates into the surrounding crystals (Fig. 1A). The rounded edges of the pores, their identical size to that of G20 cells (width $= 0.3 \pm 0.1$ µm, median $= 0.3$ µm, length $= 0.7 \pm 0.4$ µm, median $= 0.6$ µm, $N = 93$), the ~10 µm long or wide dendritic and swirling aggregates, and the occasional presence of cells within the pores indicate that these features are sections through the casts of G20 cells (Fig. 1A). Conversely, rare, < 1 µm thick pores in the sterile calcite crusts are present only at the boundaries between crystals, mainly as < 0.2 µm thick lines (Fig. 1B). These pores have geometric edges outlined by the faces of adjacent crystals and do not form dendritic or swirling patterns (Fig. 1B).
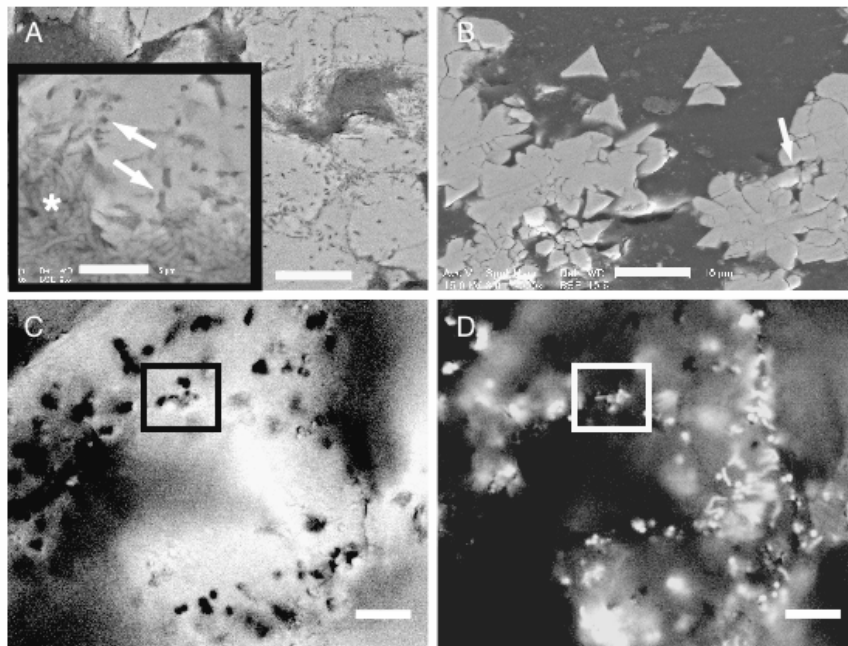
Figure 5-1   Calcite crusts precipitated in laboratory. Unless otherwise stated, scale bars in all images represent 10 µm. A: Backscattered SEM image of a dense cluster of

G20 cells in a cavity of a old crust. Inset: An enlarged view of G20 cells (asterisk) and micropores (arrows) in calcite precipitate; scale bar represents 5 μm. Cells have an enhanced contrast, having been postfixed with OsO_4. B: Backscattered SEM image of a crust precipitated in absence of bacteria. Arrow indicates abiotic micrometer-scale pores. C: Transmitted-light plan view of a crust formed in presence of G20. Round black features are pores (e.g., in black square). Focusing up and down on different depths within same sample shows that pores are present at multiple levels within crusts. D: Fluorescent-stained G20 cells in same field of view as in C (white square). As in C, square shows only some of cells; more are detected by focusing up and down.

The biologically produced pores in the SEM images are consistent with the distribution of G20 cells as shown by confocal microscopy: G20 cells are present in sparse monolayers rather than as continuous biofilms, whereas dense cell aggregates are present only in the cavities and depressions within the crusts (Figs. 2 and 3). The cells are much more abundant in the cavities probably because other areas fill in quickly with calcite that precludes the continued growth of bacteria. Consequently, pores are abundant around cavities but barely noticeable within sparsely colonized spar crystals.

Micropores can also be detected by transmitted-light microscopy (Fig. 1C). To confirm the correlation between the G20 cells and the micropores, we stained the cell membranes and observed collocalized G20 cells and pores (Fig. 1D). Neither pores nor stained cells are observed in the abiotic crust samples.
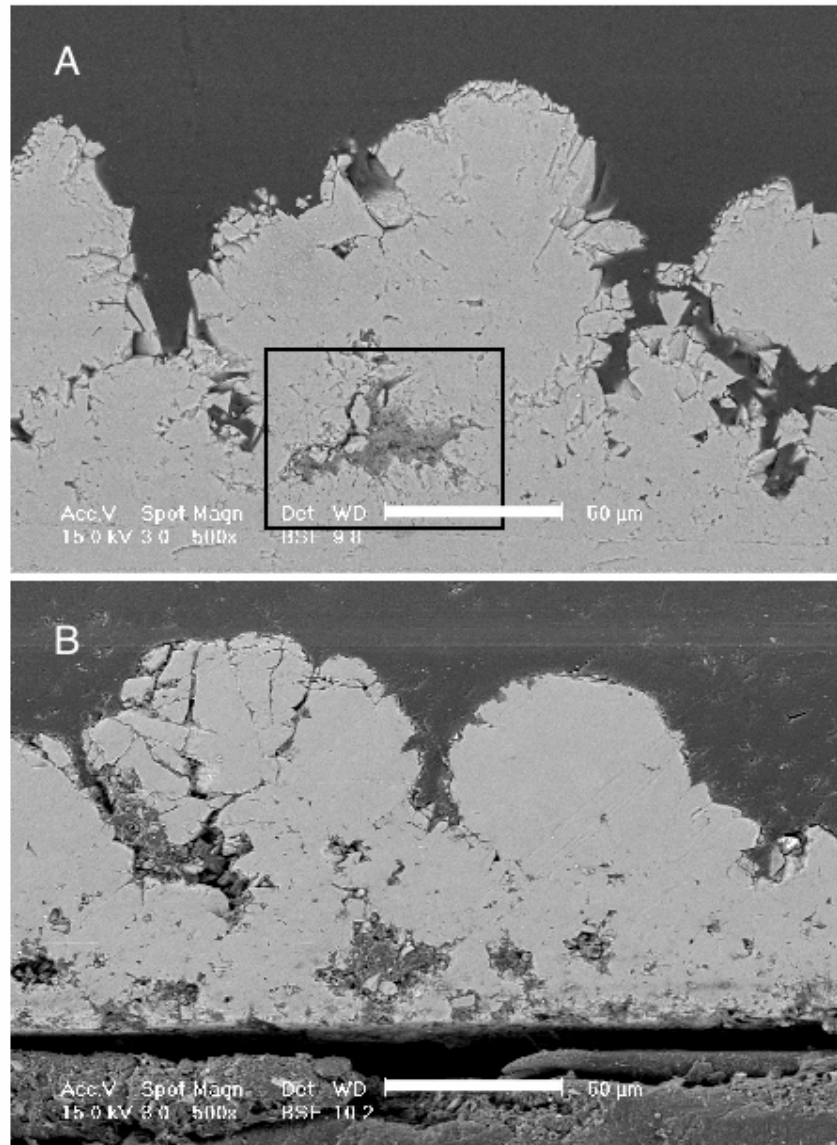
Figure 5-2   Backscattered SEM images of 4-day-old crusts (vertical cross section) precipitated in laboratory. Scale bar represents 50 μm. A: Crusts precipitated in presence of G20. Black rectangle shows a region with abundant micropores. B: Crusts precipitated in absence of bacteria.
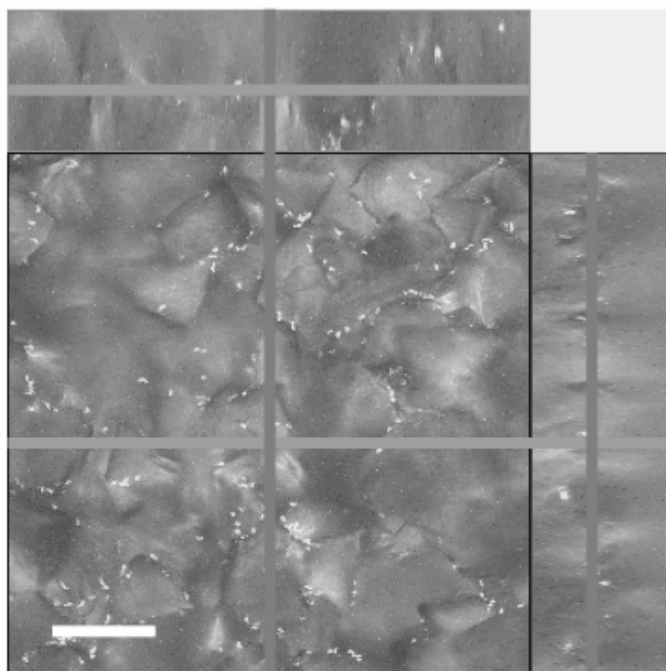
Figure 5-3   Confocal image of sparse G20 cells on top of 3-day-old crusts. Scale bar represents 30 μm. Confocal images of G20 cells (white) are combined with transmitted-light image of crust. Central part is plan view (*x-y* plane), and side images are vertical cross sections through crust (light gray line is *x-z* plane and dark gray line is *y-z* plane). Confocal images of fluorescent-stained cells were taken by a Zeiss 510 LSM at Biological Imaging Center of Beckman Institute at California Institute of Technology.

Micropores in a Modern Alkaline Environment

To see whether our laboratory experiments were applicable to the field, we searched for micropores in carbonate crusts precipitated in the waters flowing through ultramafic rocks near Cazadero, California, USA, pH ≥ 11 (Fig. 4A, [111]). The high pH at the site (pH > 11) likely precludes the growth of abundant microorganisms because

only a few extremophiles have such high-pH growth optima [112]. Although the growth rates of the carbonates remain to be determined, the fact that the crusts are commonly destroyed during the winter rainy season and rebuilt during the remaining months suggests extraordinarily fast carbonate precipitation.

We focused our attention on two main types of precipitates that alternate within the Cazadero crusts: very thinly laminated layers that show no signs of microbial presence (lamina are generally thinner than 1 μm) and larger, ray-like crystals associated with a green endolithic community (Fig. 4A, [111]). In cross-polarized light, the finely laminated sections are composed of submicrometer-scale, acicular, radiating crystals, whereas the larger, ray-like layers form large, optically continuous crystals. The absence of pores within the thinly laminated layers (Fig. 4B) is consistent with the established absence of microbes [111], whereas some micrometer-scale pores on the edges and between the crystals in the larger, ray-like fans are most likely due to the green endolithic layer (Fig. 4C). Overall, the presence or absence of microporosity in different parts of the Cazadero carbonates is consistent with the presence or absence of microbes as suggested by our lab experiments.
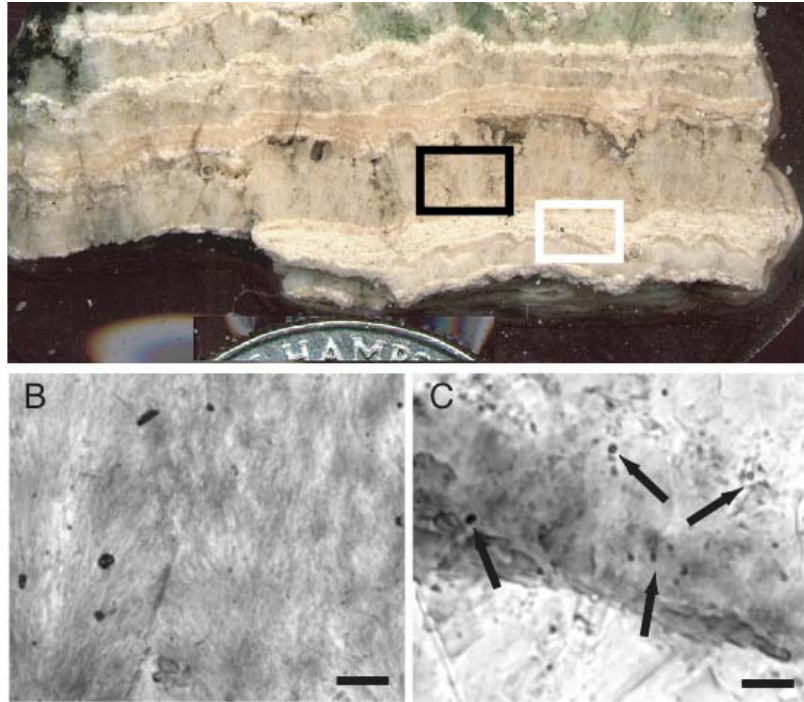
Figure 5-4 Micropores from carbonate crusts formed in a serpentine-forming environment (Cazadero, Northern California). A: Crust sample with coin for scale. White square—typical finely laminated fans; black square—typical ray-crystal crusts. B: Detail of a laminated carbonate fan. Crystals are very well preserved, clear, and compositionally banded into darker and lighter horizontal layers. Dark particles are debris that was incorporated into growing crystals. C: Detail of boundary between two ray-like crystals. Micrometer-scale pores (~1.5 μm diameter) are abundant at crystal surfaces close to boundary (arrows). Scale bars in B and C represent 10 μm.

Micropores in an Ancient Stromatolite

Having analyzed laboratory and modern natural precipitates, we sought to determine whether similar features could be found in significantly older rocks where

reprecipitation and recrystallization may alter the original carbonate fabrics. A columnar stromatolite composed of calcium carbonate (ca. 544 Ma in age) was chosen from the Precambrian-Cambrian transition near Mount Dunfee, Esmeralda County, Nevada. Although composed of calcium carbonate, the Mount Dunfee stromatolite formed in a predominantly siliciclastic paleoenvironment, suggesting that in situ precipitation of carbonate grains was stimulated biologically instead of being abiotic (e.g., [1]). The stromatolite laminae and cements display dull to moderate luminescence under cathodoluminescent examination. Therefore, we suspect that the sample has undergone some postdepositional recrystallization typical of rocks of this antiquity, and the results presented here should be treated with a degree of caution. Despite moderate diagenetic alteration, we found rounded (~ 0.5 to 1 μm in diameter), micrometer-scale pores in the carbonate crystals that define lamina within the Mount Dunfee stromatolite (Fig. 5A and 5B). Although we could not detect dendritic patterns, the abundance of intraparticle micropores within large calcium carbonate crystals and the absence of zonation are consistent with a biogenic origin. It is important to note that carbonate cements in adjacent sandstone that precipitated later in the paragenetic sequence revealed far fewer inclusions of this kind, further supporting interpretation of the micropores as biogenic (Fig. 6). We view the presence of the micropores as corroborating evidence, but not proof, that microbes were present during the construction of the stromatolite.
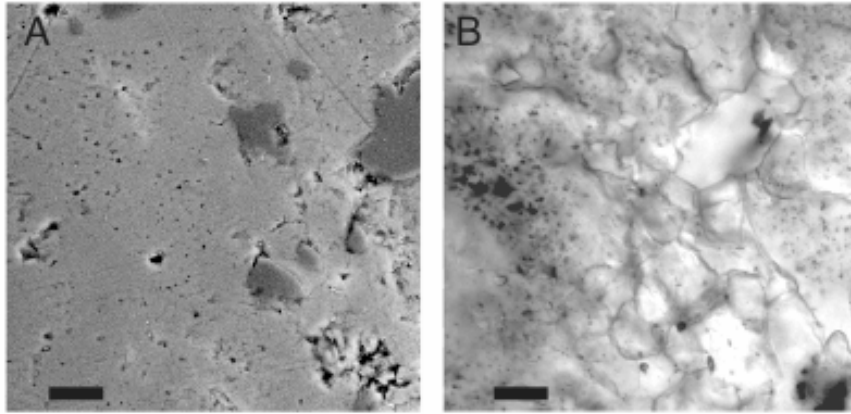
Figure 5-5   Micropores in a small bioherm of carbonate stromatolites in shale matrix (Deep Spring Formation, Mount Dunfee, Esmeralda County, Nevada). Scale bars represent 10 μm. A: Backscattered SEM image of a polished thin section of a stromatolite; 0.5–0.8 μm diameter pores are abundant in carbonate crystals (light areas) and absent from Si-Al–rich areas (dark grains), identified by EDS (energy-dispersive spectrometry). B: Transmitted-light image of same field of view as in A. Pores visible are not limited to crystal surface because light-microscopy samples a much larger depth than SEM.
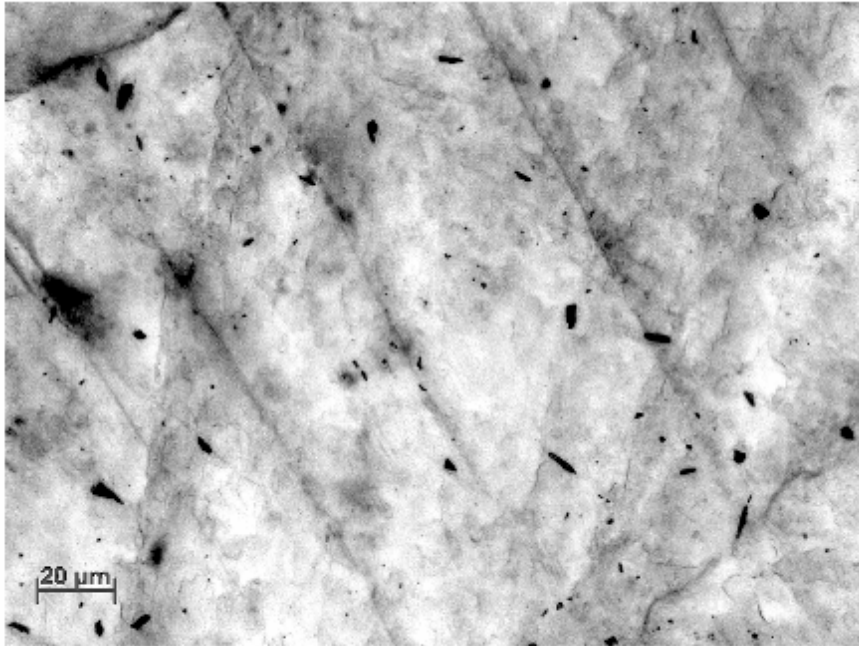
Figure 5-6 Transmitted-light image of pore-filling carbonate cement within a cavity of Mount Dunfee stromatolite sample (at approximately the same scale as Fig. 5-5). There are inclusions, but they are generally large and shaped like mineral grains. Prominent lineations oriented across thin section are calcite cleavage planes. Scale bar represents 20 μm.

Discussion

Abiotic and Microbial Processes That Create Porosity in Carbonate Rocks

Abiotic processes that interfere with crystal growth can create primary microporosity [113] that might be confused with biogenic microporosity. However, primary porosity and, particularly, secondary porosity (due to postdepositional

dissolution, dolomitization, brecciation, or fracturing) commonly produce crystallographically controlled zoned pores associated with intergranular spaces, fractures, and rhombic dolomite crystals [113, 114]. Similarly, primary abiotic porosity in our experimentally produced samples consists of recognizable polygonal interparticle spaces (Fig. 1B). In contrast, micropores experimentally produced by G20 are present throughout crystals. These micropores mirror the shape and size of G20 cells, form swirling or dendritic patterns that can be related to the spatial arrangement of cells attached to the growing crystal surfaces, and are not distinctly zoned.

G20 cells appear to create micropores by preventing calcite precipitation in their immediate neighborhood (which is also consistent with the absence of crystals within the dense G20 aggregates in Fig. 1A) and not by metabolic stimulation of calcium carbonate precipitation (as in, e.g., [115, 116]). Because G20 micropores form as the crystals precipitate, they cannot be attributed to postdepositional endolithic activity (e.g.,[117];[111];[101]). Endolithic bacterial borings are concentrated around the crystal edges, form tubular networks, often appear to follow a specific crystallographic direction ([117], [118]; Fig. 9B of Vogel et al. [101]), and are thus morphologically distinct from G20 micropores. These findings reiterate an important but often neglected point: microbial morphological signatures such as fossilized cells or micropores in carbonate rocks tell us only that cells or biofilms existed on the growing surfaces and do not imply that a particular active metabolism or behavior was responsible for the formation of the same rocks [1].

Possible Relationships Between Crystal Growth Rates and Biological Microporosity

We suspect that the formation and preservation of micropores depend on a delicate interplay between the rate of carbonate precipitation and biofilm formation. The densest micropores are present around large cellular aggregates in the cavities within the crusts, but few pores are found associated with sparse G20 monolayers (Figs. 2 and 3). Therefore, if crystal growth matches or exceeds the pace of recolonization by the biofilm, many crystals could remain uncolonized and devoid of micropores (Fig. 1A, Ref. [88]). However, the existing micropores are not filled in because the cells start decaying after being rapidly and completely embedded in crystals (i.e., inaccessible to the calcium- and carbonate-bearing fluid). A compact, fast-accreting matrix such as travertine [51, 119] is therefore more likely to preserve recognizably biogenic pores against cementation than a slowly accreting carbonate deposit in modern marine settings [120]. Consequently, an abundance of micropores in single crystals within ancient putative microbialites would be consistent with fast crystal-growth rates. These hypotheses can be tested in laboratory studies of the interactions of a variety of microorganisms with crystals and crusts growing at different rates.

Conclusions

Our experimental work demonstrates that micrometer-scale porosity can indicate microbial presence in carbonate structures. Such a biomarker should be particularly useful in environments where life is sparse and other biomarkers (e.g., isotopic, organic

remnants) are not abundant. Morphological criteria by which to recognize biogenic micropores in recent and well-preserved samples include the following: (1) the sizes and shapes of micropores mirror the sizes and shapes of microbes present during accretion of the carbonate matrix; (2) micropores form around larger cavities where dense microbial aggregates can develop; (3) the micropores are distributed throughout the crystals instead of being zoned and limited to the crystal edges; (4) the micropores show a similarity to "inclusions" under transmitted light. Together, these criteria suggest that "inclusions" with similar shape, size, and distribution in many petrographic thin sections may be biogenic. Accordingly, a systematic examination of previously ignored micropores in stromatolites and other presumed microbialites may inform our search for evidence of early life on Earth.

6. Conclusions and Implications

Can laboratory experiments such as the ones described in the previous chapters help us hear what the old rocks say to us? What caveats should we be aware of before we use the results of the reductionist approach to interpret structures that may reflect a wide range of physical, biological and chemical parameters? The ability to manipulate simplified systems enabled us to challenge a commonly held assumption about the importance of a particular metabolism, sulfate reduction, in the formation of calcium carbonate minerals in the ancient oceans. The controlled simultaneous precipitation of carbonate crusts in the presence and absence of microbes was key to distinguishing between abiotic and biologically-produced morphological signatures, as exemplified by micropores and peloids. The simplified systems thus enabled us to chemically simulate environments that may not be found on modern Earth, or may not allow controlled manipulation.

Previous chapters describe the fundaments of an experimental system where chemical and biological parameters can be monitored and changed. Future iterations of these systems should involve the ability to continuously monitor chemical conditions. pH and the partial pressure of CO_2 are examples of chemical parameters that should be constantly monitored or easily maintained or changed. So far, we performed most of our experiments under a very high partial pressure of CO_2, in solutions with high concentration of DIC (> 50 mM), and at fairly high precipitation rates. These conditions resulted in the growth of large calcite crystals on the scale of tens to a hundred micrometers, as opposed to < 10 μm crystals precipitated when the DIC content was low (~ 8 mM). Consequently, we predict that there will be significant textural differences

between these carbonate crusts and long-term carbonate precipitates formed at lower partial pressure of CO_2, an overall smaller DIC content, and lower precipitation rates that would simulate progressively younger oceans.

Our observations in the long-term precipitation experiments suggest that, even when microbes are not crucial for mineral precipitation, their morphological imprint will depend on the shape and size of their cells and the ability to colonize the accreting carbonate structures. Because our approach is limited to few cultivable model organisms with representative metabolisms in place of hundreds or thousands of species and chemical microniches that coexist within natural sediments, our model systems inevitably fail to reproduce the morphological and physiological diversity of the natural microbial communities. Even so, we have barely begun to explore the morphological signatures of cultivable species by comparing and contrasting the morphological imprints of various microbes in the sedimentary textures. The laboratory-based approach enables us to examine the morphological input of often-overlooked organisms such as anoxygenic phototrophs that do not dominate modern natural stromatolites, but may have dominated very ancient sediments before the evolution of oxygenic photosynthesis. The initial steps in this direction are described in Appendix 1.

Ultimately, the laboratory-based approach is meant to complement the observations from the natural environment and inspire new experiments with natural systems. For example, our experiments show that bacteria kinetically stimulate calcium carbonate precipitation even under the conditions where the equilibrium models of mineral precipitation do not predict a significant stimulation. Follow-up laboratory experiments can point to the kinetic inhibitors and active metabolic processes that could

be expected to stimulate or inhibit mineral precipitation in natural environments. For example, it is still unclear why the micritic carbonate layers appear primarily in association with the sulfate-reducing layers of some modern stromatolites [5], instead of being associated with the layers of anoxygenic or oxygenic phototrophs, organisms that can induce much larger shifts in the SI of modern seawater. The ongoing comprehensive tracking of the processes within various metabolic niches, analyses of the organic and inorganic kinetic inhibitors and studies that link mineral precipitation to the metabolic processes and specific physiologies could design experiments to answer similar remaining questions inspired by laboratory observations [2, 5, 44, 120-122]. Laboratory studies of the behavior and mineral-precipitating capability of real complex communities in response to the varying concentrations of sulfate, DIC, calcium, nitrogen, phosphorus and other parameters constitute another approach that would bring the laboratory models closer to nature. Among other information, these experiments and systems could determine the isotopic composition of carbon in the organic matter and the concurrent precipitates under variable conditions representative of the evolving ancient oceans and compare it to the isotopic signatures in ancient stromatolites.

This by no means exhausts the list of experiments that test the relationship between microbial metabolisms, physiologies, lithification and the ultimate morphology of stromatolites and other microbial carbonates. Although realistic models of the microbial responses require bringing the laboratory closer to natural systems, studies of some macroscopic microbial behaviors with analogs in the rock record require a reductionist approach. Chapter 7 is an example of a proposed study that would link the

unique multicellular macroscopic behavior of some cyanobacteria to its molecular basis,

and to the rock record.

7. Future work

By simulating the early oceans, growing microbial biofilms and forming baby microbialites in the laboratory, I investigated chemical and physical conditions that lead to the preservation of microbial signatures in rocks. Beside the question of how and when communities lithify, an equally fundamental problem that needs to be addressed before we can use morphology as a biomarker is what determines the shape and the fairly regular spacing between modern cyanobacterially-dominated aggregates (Fig. 1). In my postdoctoral research, I hope to focus on genes that control the macroscopic shape and scales of cyanobacterial aggregates (biofilms) and test how these aggregates respond to environmental stimuli such as light or nutrients.
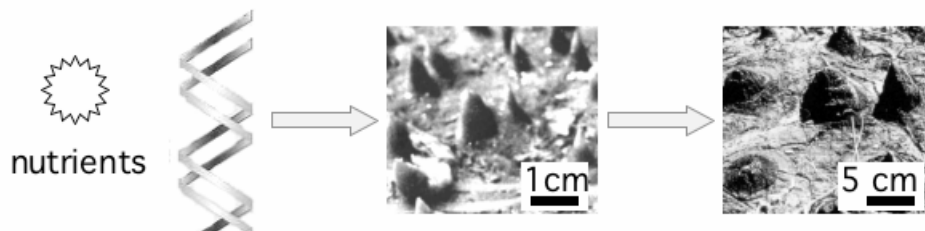
Figure 7-1   Some features in the rock record may reflect genetically encoded macroscopic behavior of microbial cells. Genes determine the cyanobacterial response to environmental stimuli such as light and nutrients (left) and regulate the microbial cell cycle. Cm-scale conical aggregates by *Phormidium tenui* in microbial mats [123] may form by chemotactic or phototactic responses to either environmental stimuli or as a manifestation of multicellular development cycle (middle). 1.6 billion years old, cm-scale conical stromatolites may preserve this behavior (right).

Ancient stromatolites by and large formed in shallow marine settings. The early rise of photosynthesis and the still uncontested molecular biomarkers imply that cyanobacteria and their anoxygenic ancestors dominated shallow coastal environments where stromatolites are found. Moreover, modern benthic cyanobacteria have been long known to aggregate into millimeter- to almost decimeter-sized cones, tufts, bulbs and spherical structures whose scales and shapes resemble some ancient stromatolites (Fig. 1) [123, 124]. All these arguments support a role for ancient photosynthetic organisms in the formation of stromatolites, but it is unclear whether different shapes of stromatolites reflect the colonization by different (cyano)bacterial species, microbial metabolisms, lithification processes, the precipitation rates of calcium carbonate, or local currents and waves.

How genetically identical cells form complex spatial patterns, what processes set the scale of these patterns and how the patterning is regulated at the molecular level is a question that unites geology and developmental biology [125]. Even seemingly simple systems can develop complex patterns, as shown by the studies of chemotactic response of *E. coli* [126-128]. By studying pattern formation in more geologically relevant model organisms, I hope to explore the differences determined by the cell size and shape (long filaments as opposed to small rods), type of motility (cyanobacterial gliding as opposed to the swimming of *E. coli*) and environmental controls that fuel the metabolism (light as opposed to organic compounds). The small pinnacles formed by *Phormidium tenui* (Fig. 1) may reflect a unique confluence of phototaxis, tangling of the filaments, and diffusion of a cell-density dependent chemical attractant. A knowledge of parameters and genes that lead to specific size cones or the spacing between the cones will help us understand

what makes similar shapes in rocks uniquely biogenic. Given that many cyanobacteria undergo morphological differentiation into vegetative cells and N-fixing heterocysts [129-131], an even more intriguing question arises by looking at the coniform and other morphologically complex structures formed by cyanobacteria. Could these three-dimensional structures reflect a genetically encoded developmental program? Complex social behavior that results in morphologically differentiated multicellular aggregates is certainly not without precedents in the prokaryotic world [132].

The field of multicellular microbial aggregates has experienced tremendous progress in the past decade, and, not surprisingly, medically important heterotrophic organisms often took the spotlight of this research [133-135]. These organisms and biofilms, however, may not be good model organisms for the ancient coastal biofilms. By using mutants of genetically tractable cyanobacteria (e.g., *Synechococcus* PC6803 or *Anabaena variabilis* ATCC 29413) to study pattern formation by cyanobacterial colonies and biofilms, I hope to bring attention to the morphologically important peculiarities of cyanobacterial biofilms. Some obviously relevant mutants to explore are those that involve motility, photosynthesis and phototactic response [136-138]. The importance of cell-density dependent signals [139, 140] and cellular differentiation in the spatial organization and behavior of photosynthetic biofilms is an equally intriguing question to investigate [141].

A major obstacle in the studies of cyanobacterial genetics has been the lack of reliable methods by which to transform cyanobacterial cells. Most attempts of transformation have, however, targeted the free-living marine cyanobacteria. By learning the genetic techniques in genetically tractable cyanobacteria, I would like to develop a

genetic system for a morphologically distinct cyanobacterium (e.g,. a *Phormidium* spp.). Using both biochemical and genetic tools, I hope to probe complex cyanobacterial structures for signs of morphological differentiation (e.g., [142]).

An important goal of this research is to bring the organisms and genes back to the context of their physical, chemical and ecological environment (in mixed model communities) and evaluate the effect of interesting controllable phenotypes in precipitation and fossilization experiments. Some examples of more geologically oriented and inspired questions that can be answered in model systems are: How mutants with a changed sensitivity to light or motility recolonize the growing precipitates relative to wild type cells, how the environmental chemical cues and conditions relevant for the early oceans (low phosphate and nitrate) trigger the multicellular organization and affect the mineral formation within model communities.

Appendix 1. Stimulation of calcite precipitation by anoxygenic photosynthesis in a high-DIC medium

Introduction

Two main observations are used as the arguments in favor of cyanobacteria as the primary architects of both ancient and modern stromatolites. First, ancient stromatolites were most common in shallow marine settings, nowadays inhabited by light-dependent carbonate secreting organisms such as corals, foraminifera, or, more rarely, by stromatolite-building cyanobacterial communities. Second, old stromatolites are occasionally similar to some modern cyanobacterial aggregates at a cm-to-dm scale.

A more careful consideration of microbial diversity and the rock record suggests that processes and organisms that build modern stromatolites may not be an adequate analogue for the ancient structures. For example, the oldest stromatolites (3.45 billion years old) appear before the first putative biomarkers for cyanobacteria, and certainly before the rise of atmospheric oxygen. It is thus possible and likely that organisms performing anoxygenic photosynthesis built stromatolites even before oxygenic photosynthesis appeared on Earth [143]. As for the morphological similarity between modern cyanobacterial structures and some ancient stromatolites (e.g., [123, 124]), there are no mechanistic models that explain how either these organic or fossilized conical shapes are built, and whether they could be only built by photosynthetic organisms. Lastly, even the coarse lamina of modern stromatolites built by cyanobacterial trapping and binding of the sediment are in replaced by fine lamina formed by *in situ* precipitated

carbonate minerals as we go further back into the rock record. The change in the mechanism by which stromatolites accreted is consistent with a higher supersaturation state of the oceans with respect to calcium carbonate. Modern highly supersaturated environments analogous to the Precambrian marine settings are mainly oxic, and dominated by cyanobacteria whose role in the precipitation of calcium carbonate minerals and the formation of modern stromatolites received considerable attention [49, 115, 120, 144]. The contribution of potentially more relevant anoxygenic photosynthetic bacteria to the formation of ancient stromatolites is, however, poorly understood.

Anoxygenic photosynthetic bacteria use various inorganic and organic compounds as electron donors to inorganic carbon, many of which, such as iron(II), reduced sulfur compounds, and molecular hydrogen, could have been present on an anoxic early Earth before the rise of oxygen. Eq. 1 and Eq. 2 describe photosynthetic growth with molecular hydrogen as an electron donor:

$$2H_2 \rightarrow 4H^+ + 4e^- \tag{3}$$

$$HCO_3^- + 4e^- + 5H^+ \rightarrow CH_2O + 2H_2O \tag{4}$$

The photosynthetic uptake of inorganic carbon increases the concentration of carbonate ion (Eq. 3).

$$2HCO_3 \leftrightarrow CO_3^{2-} + CO_2 + H_2O \tag{3}$$

The increase in carbonate concentrations drives the precipitation of calcium carbonate (Eq. 4) because it increases the saturation index (SI) of calcite (Eq. 5).

$$Ca^{2+} + CO_3^{2-} \rightarrow CaCO_3 \tag{4}$$

$$SI = \log \frac{[Ca^{2+}][CO_3^{2-}]}{K_S} \tag{5}$$

where K_s is the solubility constant of calcite.

The increase in the concentration of carbonate ion and local pH changes induced by oxygenic phototrophs in modern freshwater and some marine settings can significantly stimulate the precipitation of calcium carbonate, because these environments are poorly buffered by DIC [145]. In contrast, the increase in the concentration of carbonate ion associated with photosynthesis is not predicted to have a large effect in the environments with a high concentration of DIC due to the large pool of inorganic carbon, and the strong pH buffering [52]. The growth of anoxygenic phototrophs on hydrogen as described by Eq. 1 and Eq. 2 results in the same net production of carbonate ions as oxygenic photosynthesis, and would be predicted to have the same net effect on the precipitation of calcium carbonate. Here we investigate the influence of anoxygenic photosynthesis on *in situ* calcite precipitation in solutions that contain a high concentration of dissolved inorganic carbon (DIC) in a modeling and experimental study of *Rhodopseudomonas palustris* strain GCA009.

Materials and Methods

Growth Medium And Conditions. We used *R. palustris* strain GCA009 (from C. Harwood's lab) as a model organism. GCA009 was grown in modified, bicarbonate-buffered photosynthetic medium, using an incandescent light bulb (75 W) as a light source. The basal medium contained: 0.3 g/L $(NH_4)_2SO_4$, 0.1 mM KH_2PO_4, 0.9 g/l KCl, 0.4 g/l $MgCl_2$, 0.1 mM $Na_2S_2O_3$, 1 ml/L of 1g/L PABA, 1 ml/l concentrated base. The concentrated base contains 20 g/L nitriloacetic acid, 28.9 g/L anhydrous $MgSO_4$, 6.67 g/L $CaCl_2 \bullet 2H_2O$, 18.5 mg/L $(NH_4)_6Mo_7O_{24} \bullet 4H_2O$, 198 mg/L $FeSO_4 \bullet 7H_2O$ and 100 ml/L

of Metal 44 solution. Metal 44 solution contains 2.5 g EDTA, 10.95 g $ZnSO_4 \bullet 7H_2O$, 5 g $FeSO_4 \bullet 7H_2O$, 1.54 g $MnSO_4 \bullet H_2O$, 392 mg $CuSO_4 \bullet 5H_2O$, 250 mg $Co(NO_3)_2 \bullet 6H_2O$, and 177 mg $Na_2B_4O_7 \bullet 10H_2O$ per 800 ml. The medium was boiled under nitrogen, cooled under a mixed atmosphere of 80% N_2 and 20% CO_2, amended with 40 ml of *1M* $NaHCO_3$ from sterile stock solution and left to equilibrate with an atmosphere of 80% N_2, 15% CO_2 and 5% H_2 (adding to 1 atmosphere total) for at least one day. The pH was adjusted by 10 *N* NaOH to 7.4 -7.5, and the medium was filter-sterilized by a 0.2 μm filter and stored in the anaerobic glove box for at least a week before it was used in the experiments. All the glassware used in the experiments was stored in the anaerobic glove box for at least a week before it was used in experiments. Different light intensities were obtained by moving the cultures toward or away from the light (making sure that the temperature was constant). The light intensities were measured by a dual-range lightmeter Traceable® by Control Company, Friendswood, Texas. The growth rate at 280 lux was measured by daily cell counts of DAPI-stained cells from triplicate tubes. The growth rate at 580 lux was not measured, but we noted that the same optical densities at this light intensity were reached in considerably shorter time.

Precipitation experiments. Mid-exponential phase cells (cell density 1 x 10^8 cells/ml) grown photosynthetically on hydrogen were centrifuged anaerobically to remove the liquid phase. The bacteria were inoculated into 2.5 ml of the fresh culture medium in triplicate sterile screw-capped glass tubes to a cell density of 1.4 x 10^8 and 1.4 x 10^9 cells/ml (the latter corresponding to the early stationary phase cell density). To distinguish between the influence of actively photosynthesizing cells and the influence of inactive cellular material on calcite precipitation, we inoculated triplicate glass tubes to a

cell density of 1 x 10^8 cells/ml and wrapped them completely in aluminum foil. We added 2.5 ml of sterile culture medium to three glass tubes as sterile controls. After inoculation, $CaCl_2$ was added to sterile controls and cultures to 12 m*M* final concentration from a sterile 1*M* stock solution. The glass tubes were incubated at 25°C and at the light intensity of 280 and 570 lux, respectively. We determined the amount of precipitate by taking 120 l samples every two days, filtering them anaerobically, adding 100 l of the filtrate to 10 ml of 1% HNO_3 and measuring the calcium concentration by inductively coupled plasma mass spectrometry (ICP-MS) at the Analytical Facility at Caltech. The alkalinity of the experimental solutions was determined by Gran-titration of 10-ml aliquots using 0.8 M H_2SO_4. Visual observations of the crystals in the 8-well LabTek® (NalgeNunc International) chambered culture dishes with coverslip bottoms confirmed that the decreasing calcium concentrations could be attributed to the precipitation of calcite crystals. The crystals in each well were point-counted microscopically after four days. The crystal structure of the precipitates was determined by X-ray diffraction using a Scintag diffractometer with Cu K (= 1.5405 Å).

Precipitation in the reactors. Two identical 9 cm diameter, ~ 40 ml working volume sterile glass reactors containing sterile plastic chips were preincubated for a week in the anaerobic glove box under an atmosphere of 82.5 % N_2, 15% CO_2 and 2.5% H_2. The reactors were inoculated with 5 ml of a mid-exponential culture of GCA009 into 30 ml of the medium of the same composition as described above. One reactor was set to receive 580 lux, while the other was shaded down to 290 lux and the GCA009 biofilms were allowed to establish themselves for a week. Two batches of the basal medium were made with the same composition of basal ions as described above. One batch contained 20 mM

of CaCl$_2$ from the 1 M anaerobic stock solution, but was not amended with NaHCO$_3$ from, while the other one was amended with 80 mM of sterile NaHCO$_3$ from 1 M anaerobic stock solution and no calcium. The solution containing CaCl$_2$ was flushed with pure N$_2$ and the bicarbonate containing solutions was flushed with a gas mix containing 80 % N$_2$ and 20% CO$_2$ for three days. The pH of the two solutions was then adjusted to 7.4 and 7.8, respectively and they were filter-sterilized. After one week of GCA009 biofilm growth, the medium in the two reactors was removed completely and replaced by the 1:1 mixture of the Ca-containing and bicarbonate-containing media. The plastic chips covered by biofilms and precipitates were removed weekly from both reactors and fixed in Karnovsky fixative after collection [90]. The cell density in each reactor was measured either by measuring the optical density at 470 nm by a spectrophotometer in aliquots of the cultures from the reactors, or by direct microscopic counts of DAPI-stained cells. 15 ml aliquots of the culture medium from both reactors were used to determine the alkalinity of the solutions before each medium exchange by Gran-titration. The alkalinity of the replacement solution was determined each week in a 1:1 mixture of the Ca-containing and bicarbonate-containing media.

Geochemical modeling. Chemical parameters such as supersaturation and concentrations of chemical components in the medium were calculated using MINEQL+ (Environmental Research Software). We assumed a closed system and modeled the photosynthetic uptake of CO$_2$ as the parallel uptake of total DIC and protons. The model solution had basal ion concentrations equal to our freshwater culture medium (see above) and with 10 m*M* CaCl$_2$. The pH of the model medium was adjusted by the addition of LiOH or HNO$_3$. Table 1 summarizes the composition of the medium as used in the modeling

studies. The calcite saturation constant used by the program is $K_s = 10^{-8.48}$ and the software calculated the ionic strength of the medium from the supplied concentrations of the ions in the medium, adjusting the equilibrium constants accordingly. The differential equation describing how the total carbon concentration depends on diffusion and microbial carbon fixation was numerically solved for different geometries using Partial Differential Equation Toolbox in Matlab (The MathWorks).

Results

Investigating the role of modern stromatolite-builders in solutions relevant for the Precambrian oceans, we established that calcite precipitation in high-DIC solutions was not driven by the metabolic activity of sulfate reducing bacteria, but was more consistent with the stimulation of calcite nucleation on microbial surfaces and extracellular components [8]. Chemical modeling indicated that hydrogen-based photosynthesis has the potential to stimulate the precipitation of calcite by taking up carbon dioxide even in high-DIC solutions (Figure 1). We assumed the uptake rates of 1 m*M* and 5 m*M* of CO_2 per day (within the biofilm), consistent with the estimates of carbon fixation from modern-day hypersaline microbial mats[1] [146] and lower than the > 10 m*M* of fixed C/day measured in pure cultures of photosynthetically grown *Rhodobacter sphaeroides* and *Rhodospirillum rubrum* [147] and DIC-enriched modern microbial mats [148]. Photosynthetically induced increase in the SI of calcite and the local decrease in DIC will depend not only on the biological rates of carbon fixation, but also on the actual physical

---

[1] The measured photosynthetic CO_2 uptake rate was ~ 100 nm C/cm^2/hr. Assuming a ~ 1 – 10 mm thick biofilm, this translates to a fixation rate of 1 – 10 mmoles C/L/day.

setting (Fig. 1B). Generally, photosynthesis is more likely to stimulate calcite precipitation when the rates of carbon fixation are high, and the solution is not being reequilibrated with an external source of DIC by mixing (Fig. 1).
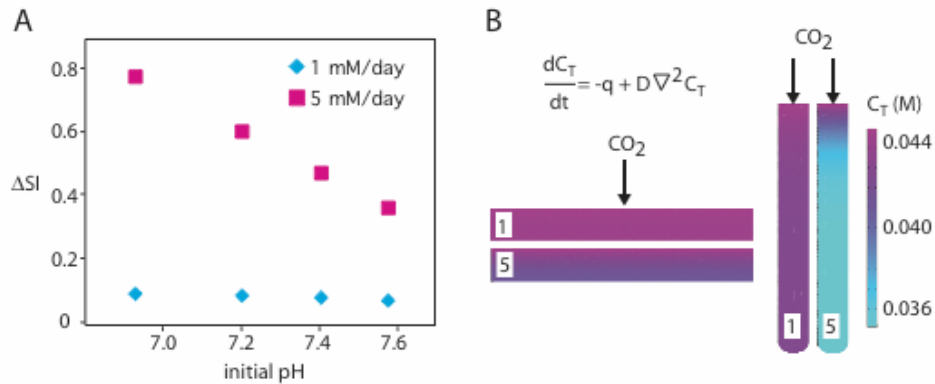
Figure A1- 1 The effect of photosynthetic rate of carbon uptake on the SI of calcite and the total concentration of DIC in the solution. A. The increase in SI due to the uptake of 1 mM (blue rectangles) and 5 mM (pink squares) of DIC in a closed system at different initial pH values (x-axis). The solution before the carbon uptake is equilibrated with 0.15 atm CO_2 and its DIC content increases with an increasing pH. An increasing DIC content increases the buffering and reduces the SI increase at higher initial pH. B. The concentration of total inorganic carbon (C_T) after 25 hours of photosynthetic carbon uptake in a 2-D diffusion model. We assumed a photosynthetic uptake rate q of 1 mM C/day ("1") and 5 mM C/day ("5"), starting with a solution in equilibrium with an infinite reservoir of CO_2 and initial alkalinity of 45 meq/L, and using $D = 2 \times 10^{-5}$ cm^2/s as the molecular diffusion coefficient of CO_2 [149]. The results are shown for two different geometries of the system: 1 cm tall x 8 cm long containers and 8 cm tall x 1 cm wide containers. In both cases CO_2 enters the solution from above (indicated by an arrow) and

the condition of no flux through the container walls is imposed on the remaining sides of the containers.

Although photosynthetic stimulation of calcite precipitation is not considered important in high-DIC shallow solutions [52], our initial visual observations revealed that the presence of GCA009 in the culture medium with an alkalinity of 51.9 ± 0.2 mM increased the number of calcite crystals by at least 5 times relative to sterile controls. The number of crystals also depended on the initial cell density of GCA009 (Figure 2).
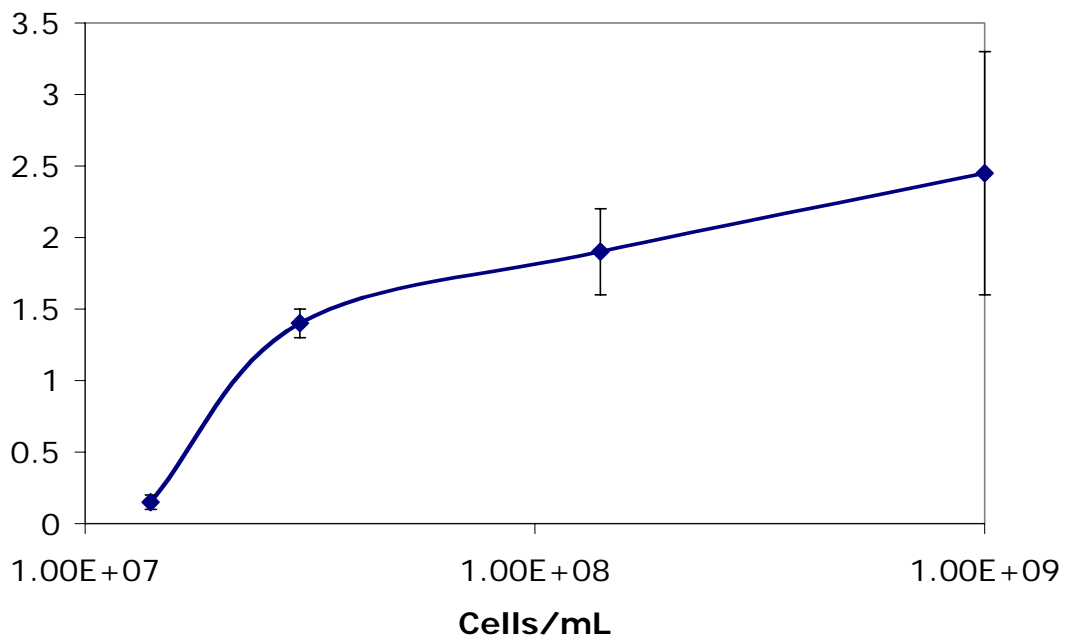
Figure A1- 2 The average number of crystals (y-axis) observed after four days in the cultures of GCA009 inoculated at different initial cell densities (x-axis). The number of crystals per field of view is the average from twenty fields of view from two independent wells in 8-well culture dishes. The highest initial cell density (10^9 cells/ml) corresponds

to the early stationary phase culture, while all the lower cell densities correspond to exponential phase cultures.

Not only nucleation, but also the total amount of precipitate appeared to be stimulated in the GCA009 cultures. We confirmed this by measuring the decrease in the total amount of calcium in the actively photosynthesizing cultures and sterile controls by ICP-MS (Fig. 3). Our previous work showed that inactive sulfate reducers and their cell membranes could stimulate calcite precipitation to an equal, if not larger, extent as metabolically active cells. To test whether GCA009 cells similarly acted as mere particles that stimulated calcite nucleation, or they metabolically stimulated the precipitation, we incubated them at two different cell densities, at two different light intensities (and, consequently, growth rates) and in the presence and absence of light (Fig. 3). The decrease in the amount of total calcium in the solution was visually correlated with the appearance of crystals in the bacterial cultures. The presence of GCA009 cells stimulated the precipitation relative to sterile controls, regardless of whether the cells were photosynthesizing or not (Fig. 3). Metabolic activity still played a role, because the precipitation started earlier in dense active cultures (regardless of the light intensity), and appeared to proceed faster than the precipitation in the dark cultures (Fig. 3). The crystals in the active cultures were larger and appeared less acicular than the crystals that grew in the dark cultures (Fig. 4).
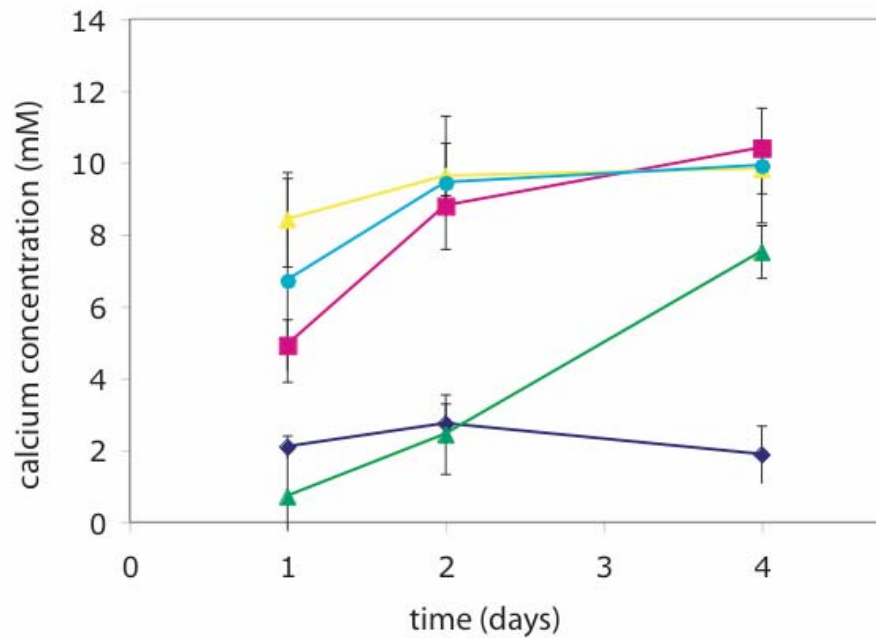
Figure A1-3 Decrease in the total concentration of calcium in GCA009 growth medium. Yellow triangles: 10^9 cells/ml initial cell density, incubated at 580 lux. Blue circles: 10^8 cells/ml initial cell density incubated at 580 lux. Red squares: 10^9 cells/ml initial cell density incubated at 280 lux. Green triangles: 10^8 cells/ml initial cell density cultures wrapped in Al-foil incubated at the same distance from the light source as the yellow triangles and blue circles. Blue rectangles: sterile controls incubated in light at 580 lux. The calcium concentration was measured in triplicate samples from independent tubes.
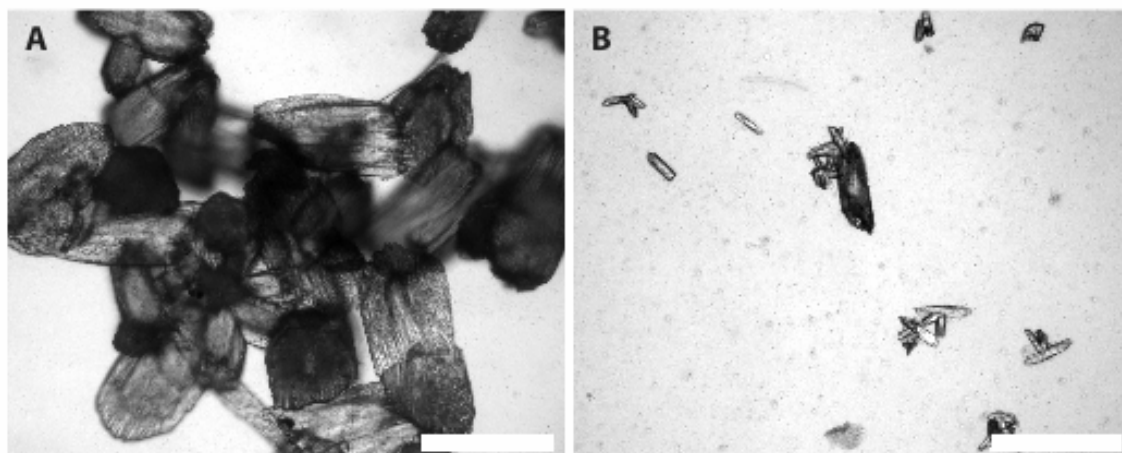
Figure A1- 3 Transmitted-light micrographs of calcite crystals from the cultures of GCA009. The scale bar in both parts is 200 μm. A. Calcite crystals that grew in the presence of photosynthetically active GCA009 cells (culture bottles exposed to light). B. Calcite crystals that grew in the presence of photosynthetically inactive GCA009 cells (culture bottles wrapped in aluminum foil).

Photosynthetically active GCA009 stimulated calcite precipitation in high-DIC solutions. This finding is in contrast to our previous experiments, where the activity of sulfate reducers was not required for the precipitation of calcite in high-DIC and low-sulfate solutions, and some accepted models for high-DIC settings [52]. Although the photosynthetic stimulation of calcite precipitation is not inconsistent with our modeling results (Fig. 1), the mechanisms responsible for this effect remain elusive. Namely, an increase in the SI of at least 0.4 log units is required for calcite to precipitate in the sterile culture medium (i.e., in the absence of cells). In a system that is not in contact with a CO_2-rich atmosphere, this increase in the SI would be accompanied by a pH increase of more than 0.5 units. However, active GCA009 stimulated calcite precipitation in loosely

capped tubes or wells were exposed to a large reservoir of CO_2, and shaken vigorously at least once daily. GCA009 cells stimulated the precipitation of calcite even in shallow cultures continuously stirred by a magnetic stir bar, opposite to the predictions shown in Fig.1. Moreover, the pH in photosynthesizing cultures never increased by more than 0.02 pH units (measured in the absence of calcium). The absence of measurable pH and SI changes in the bulk medium raises two potential explanations of why GCA009 stimulates calcite precipitation. Firstly, the pH and the SI might increase only locally, within ~ 30 μ   biofilms formed by   ˜   (Fig. 5). We hope to address this hypothesis by measuring the pH within active GCA009 biofilms using microelectrodes. Secondly, metabolically active cells can stimulate precipitation kinetically, by secreting extracellular compounds into the medium, or by taking up metabolites that kinetically inhibit calcite nucleation and precipitation (ammonia, phosphate, trace metals). Both hypotheses are consistent with the previously observed changes of calcite morphology in sulfate reducing cultures that could be explained by the uptake of nutrients and the secretion of extracellular compounds within biofilms [9]. Similar processes at the horizontal and vertical scale of single cells and biofilms are often overlooked when measuring and modeling the properties of the bulk system (in our case, the culture medium in the entire tube).

The increase in SI due to active photosynthesis is observed to lead to the formation of encrusted microbial cells only in low-DIC settings [52, 145]. Instead of being associated with microbial cells, calcium carbonate minerals in high-DIC settings are thought to be distributed randomly in the extracellular matrix [32]. Indeed, we found that the formation of large calcite crystals within either heterotrophic or phototrophic

cultures in high-DIC solutions did not seem related to the metabolically-induced changes in the saturation index (SI), and that the shape of the crystals did not reflect the shape of bacterial cells [8, 9]. However, the metabolically active photosynthetic cells significantly stimulated calcite precipitation even in the high-DIC background (Fig. 3). The absence of mineralized cells in high-DIC solutions may thus not be due to the inability of cells to photosynthetically induce mineral nucleation and precipitation in high-DIC settings [52]. More likely, the absence of mineralized cells is due to the large crystal size of the precipitates in our solutions (and in high-DIC solutions in nature, e.g., [119]). Regardless of whether the crystal nuclei form on microbial cells or in the extracellular matrix, they grow into 10-100 μm large crystals that override the shape of the micron-sized single cells. Therefore, the absence of mineralized cells may be a mere consequence of the formation of large crystals around a limited number of nuclei in a large pool of carbonate ions.
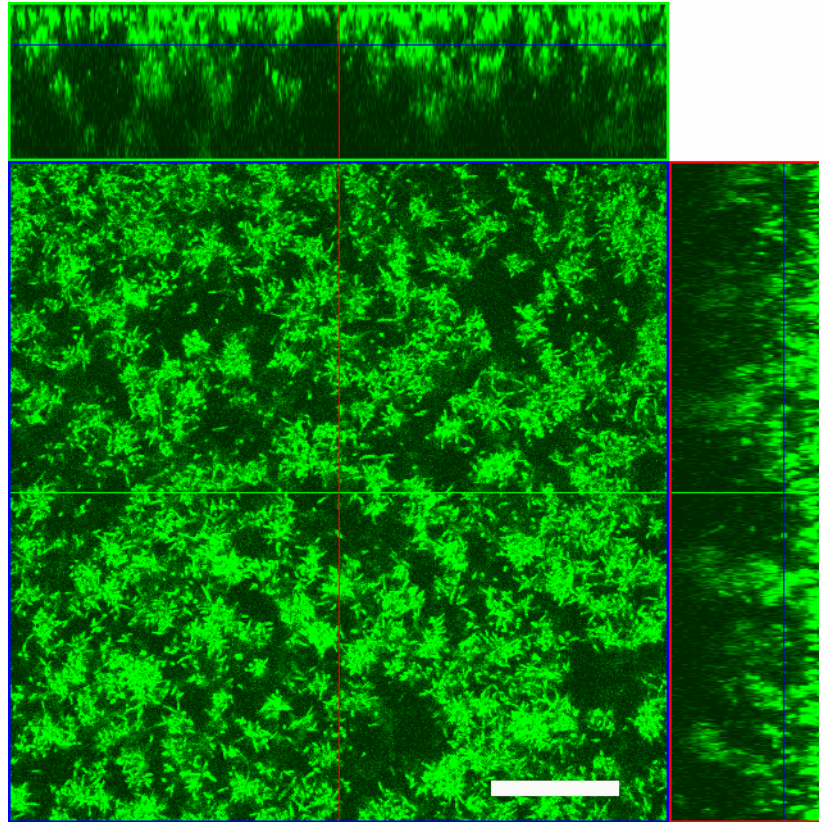
Figure A1- 4 Confocal image of a mid-exponential culture of GCA009, scale bar is 30 μm. The fluorescently stained cells (green) form ~1μm wide microcolonies and about 30 μm thick biofilms. The middle part of the image is the x-y plane at 10 μm from the bottom of the biofilm. The red line and the red sidebox show the y-z section through this plane, and the green line and the green sidebox show the x-z section through the plane of the biofilm.

The stimulation of calcite precipitation by active GCA009 biofilms can be used to address a simple hypothesis: whether different amounts of calcite crystals (Fig. 3) and their different sizes and morphologies (Fig. 4) caused by the temporal variations in the biomass and the cell activity could give rise to laminated structures. The lamination of many ancient stromatolites is commonly interpreted using models based on the behavior

of modern freshwater and marine cyanobacteria [150]. Most of these models require the presence of calcium carbonate-encrusted or sediment-trapping large (tens of m long) filamentous phototactic cyanobacteria, but it is unclear whether these organisms are required to produce lamination in sedimentary structures. By exploring the textures created by much smaller, non-filamentous GCA009 cells we hope to add a previously uninvestigated class of organisms to the parameter space of microbial morphological influences. By manipulating the cell density (Fig. 2) and the photosynthetic activity of GCA009 (Fig. 3) in calcite-precipitating cultures of GCA009, we hope to link biological processes to the amount of precipitate (Fig. 3) and the textures (Fig. 4) in the accreting Ca-carbonate crusts. The morphological imprints of GCA009 biofilms (Fig. 6) in long-term laboratory precipitates can be then compared and contrasted to the existing putatively cyanobacterial textures in the rock record.
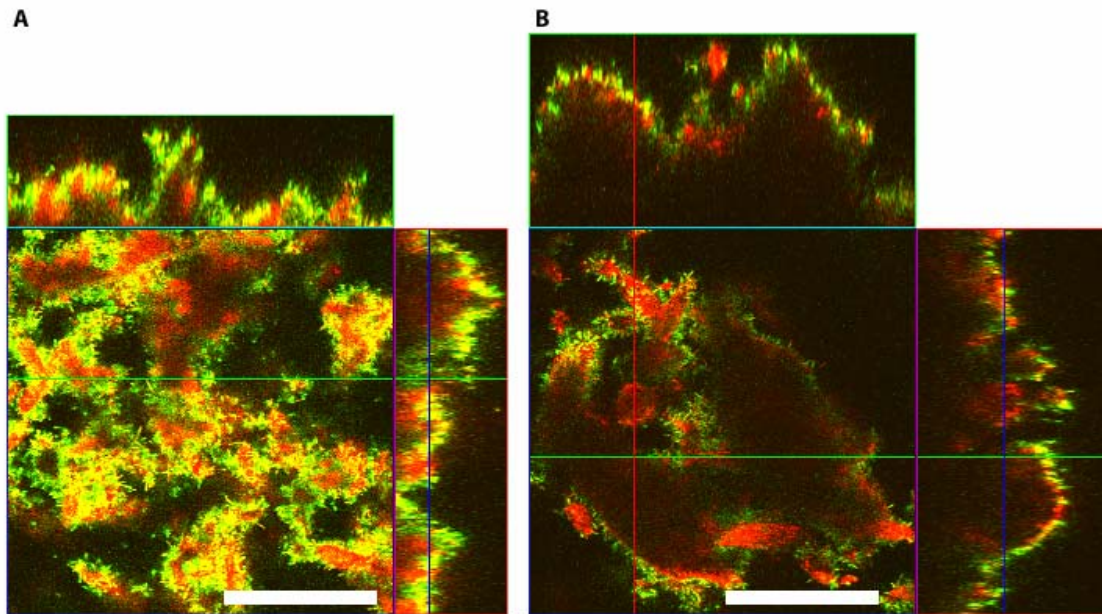
Figure A1- 5 Confocal images of fluorescently GCA009 cells (green) that grew on the calcite crystals (red) in semi-continuous cultures. The scale bar in both images is 30 μm. The central part of both images is the x-y section through the sample, and the side boxes are the y-z and the x-z sections, respectively. A. One-week old 30 μm thick sample. B. Two-week old 50 μm thick sample. The interior of this sample appears darker because of the thicker layer of precipitate that cannot be penetrated by the fluorescent light.

References

1. Grotzinger, J.P. and A.H. Knoll, *Stromatolites in Precambrian carbonates: Evolutionary mileposts or environmental dipsticks?* Annual Review of Earth and Planetary Sciences, 1999. **27**: pp. 313-358.

2. Reid, R.P., et al., *The role of microbes in accretion, lamination and early lithification of modern marine stromatolites.* Nature, 2000. **406**(6799): pp. 989-992.

3. Grotzinger, J.P., *Geochemical model for Proterozoic stromatolite decline.* American Journal of Science, 1990. **290A**: pp. 80-103.

4. Grotzinger, J.P. and D.H. Rothman, *An abiotic model for stromatolite morphogenesis.* Nature, 1996. **383**(6599): pp. 423-425.

5. Visscher, P.T., R.P. Reid, and B.M. Bebout, *Microscale observations of sulfate reduction: Correlation of microbial activity with lithified micritic laminae in modern marine stromatolites.* Geology, 2000. **28**(10): pp. 919-922.

6. Canfield, D.E., et al., *Constraining sulfate levels in Archean oceans.* Geochimica Et Cosmochimica Acta, 2002. **66**(15A): pp. A118-A118.

7. Ohmoto, H., Y. Watanabe, and K. Kumazawa, *Evidence from massive siderite beds for a CO_2-rich atmosphere before, 1.8 billion years ago.* Nature, 2004. **429**(6990): pp. 395-399.

8. Bosak, T. and D.K. Newman, *Microbial nucleation of calcium carbonate in the Precambrian.* Geology, 2003. **31**(7): pp. 577-580.

9. Bosak, T. and D.K. Newman, *Microbial kinetic controls on calcite morphology in supersaturated solutions.* Journal of Sedimentary Petrology, 2004, *in press*.

10. Bosak, T., V. Souza-Egipsy, and D.K. Newman, *A laboratory model of abiotic peloid formation.* Geobiology, 2004. **2**(3): pp. 189-198.

11. Bosak, T., et al., *Micron-scale porosity as a biosignature in carbonate crusts.* Geology, 2004. **32**(9): pp. 781-784.

12. Vasconcelos, C. and J.A. McKenzie, *Microbial mediation of modern dolomite precipitation and diagenesis under anoxic conditions (Lagoa Vermelha, Rio de Janeiro, Brazil).* Journal of Sedimentary Research, 1997. **67**(3): pp. 378-390.

13. Grotzinger, J.P. and J.F. Kasting, *New constraints on Precambrian ocean composition.* Journal of Geology, 1993. **101**(2): pp. 235-243.

14. Krumbein, W.E., *Photolithotropic and chemoorganotrophic activity of bacteria and algae as related to beachrock formation and degradation (Gulf of Aqaba, Sinai).* Geomicrobiology Journal, 1978. **1**(2): pp. 139-203.

15. Warthmann, R., et al., *Bacterially induced dolomite precipitation in anoxic culture experiments.* Geology, 2000. **28**(12): pp. 1091-1094.

16. van Lith, Y., et al., *Bacterial sulfate reduction and salinity: two controls on dolomite precipitation in Lagoa Vermelha and Brejo do Espinho (Brazil).* Hydrobiologia, 2002. **485**(1-3): pp. 35-49.

17. Wright, D.T., *The role of sulphate-reducing bacteria and cyanobacteria in dolomite formation in distal ephemeral lakes of the Coorong region, South Australia.* Sedimentary Geology, 1999. **126**(1-4): pp. 147-157.

18. Canfield, D.E. and R. Raiswell, *Carbonate precipitation and dissolution: its relevance to fossil preservation*, in *Taphonomy: Releasing the Data Locked in the Fossil Record*, P.A. Allison and D.E.G. Briggs, Editors. 1991, Plenum: London. pp. 411-453.

19. Rapp, B.J. and J.D. Wall, *Genetic transfer in Desulfovibrio desulfuricans.* Proc. Natl. Acad. Sci. USA, 1987. **84**: pp. 9128-9130.

20. Visscher, P.T., et al., *Formation of lithified micritic laminae in modern marine stromatolites (Bahamas): The role of sulfur cycling.* American Mineralogist, 1998. **83**(11-12): pp. 1482-1493.

21. Habicht, K.S., et al., *Calibration of sulfate levels in the Archean Ocean.* Science, 2002. **298**(5602): pp. 2372-2374.

22. Canfield, D.E., K.S. Habicht, and B. Thamdrup, *The Archean sulfur cycle and the early history of atmospheric oxygen.* Science, 2000. **288**(5466): pp. 658-661.

23. Anbar, A.D. and A.H. Knoll, *Proterozoic ocean chemistry and evolution: A bioinorganic bridge?* Science, 2002. **297**(5584): pp. 1137-1142.

24. Kasting, J.F., *Theoretical constraints on oxygen and carbon-dioxide concentrations in the Precambrian atmosphere.* Precambrian Research, 1987. **34**(3-4): pp. 205-229.

25. Cypionka, H., *Characterization of sulfate transport in Desulfovibrio- desulfuricans.* Archives of Microbiology, 1989. **152**(3): pp. 237-243.

26. Kroder, M., P.M.H. Kroneck, and H. Cypionka, *Determination of the transmembrane proton gradient in the anaerobic bacterium Desulfovibrio-desulfuricans by P-31 nuclear-magnetic-resonance.* Archives of Microbiology, 1991. **156**(2): pp. 145-147.

27. Chafetz, H.S. and C. Busczynski, *Bacterially Induced Lithification of Microbial Mats.* Palaios, 1992. **7**: pp. 277-293.

28. Fortin, D., F.G. Ferris, and T.J. Beveridge, *Surface-mediated mineral development by bacteria*, in *Geomicrobiology: Interactions between Microbes and Minerals*. 1997. pp. 161-180.

29. Ferris, F.G., W.S. Fyfe, and T.J. Beveridge, *Metallic Ion Binding by Bacillus-Subtilis - Implications for the Fossilization of Microorganisms.* Geology, 1988. **16**(2): pp. 149-152.

30. Mera, M.U., et al., *The Membrane-Induced Proton Motive Force Influences the Metal- Binding Ability of Bacillus-Subtilis Cell-Walls.* Applied and Environmental Microbiology, 1992. **58**(12): pp. 3837-3844.

31. Stumm, W. and J.J. Morgan, *Aquatic chemistry: chemical equilibria and rates in natural waters*. 3 ed. 1996, New York: John Wiley & Sons, Inc. 1022.

32. Arp, G., et al., *Biofilm exopolymers control microbialite formation at thermal springs discharging into the alkaline Pyramid Lake, Nevada, USA.* Sedimentary Geology, 1999. **126**(1-4): pp. 159-176.

33. Thomas-Keprta, K.L., et al., *Bacterial mineralization patterns in basaltic aquifers: Implications for possible life in martian meteorite ALH84001.* Geology, 1998. **26**(11): pp. 1031-1034.

34. Given, R.K. and B.H. Wilkinson, *Kinetic Control of Morphology, Composition, and Mineralogy of Abiotic Sedimentary Carbonates.* Journal of Sedimentary Petrology, 1985. **55**(1): pp. 109-119.

35. Gonzalez, L.A., S.J. Carpenter, and K.C. Lohmann, *Inorganic calcite morphology - roles of fluid chemistry and fluid-flow.* Journal of Sedimentary Petrology, 1992. **62**(3): pp. 382-399.

36. FernándezDiáz, L., et al., *The role of magnesium in the crystallization of calcite and aragonite in a porous medium.* Journal of Sedimentary Research, 1996. **66**(3): pp. 482-491.

37. Stumm, W. and J. Morgan, *Aquatic chemistry: Chemical Equilibria and Rates in Natural Waters*, ed. J.L.S.a.A. Zehnder. 1996, New York: John Wiley & Sons, Inc. 1022.

38. Davis, K.J., P.M. Dove, and J.J. De Yoreo, *The role of Mg^{2+} as an impurity in calcite growth.* Science, 2000. **290**(5494): pp. 1134-1137.

39. Tracy, S.L., D.A. Williams, and H.M. Jennings, *The growth of calcite spherulites from solution II. Kinetics of formation.* Journal of Crystal Growth, 1998. **193**(3): pp. 382-388.

40. Berner, R.A. and J.W. Morse, *Dissolution kinetics of calcium-carbonate in sea-water. 4. Theory of calcite dissolution.* American Journal of Science, 1974. **274**(2): pp. 108-134.

41. Buczynski, C. and H.S. Chafetz, *Habit of bacterially induced precipitates of calcium-carbonate and the influence of medium viscosity on mineralogy.* Journal of Sedimentary Petrology, 1991. **61**(2): pp. 226-233.

42. Contos, A.K., et al., *Morphoanalysis of bacterially precipitated subaqueous calcium carbonate from Weebubbie Cave, Australia.* Geomicrobiology Journal, 2001. **18**(3): pp. 331-343.

43. Braissant, O., et al., *Bacterially induced mineralization of calcium carbonate in terrestrial environments: The role of exopolysaccharides and amino acids.* Journal of Sedimentary Research, 2003. **73**(3): pp. 485-490.

44. Kawaguchi, T. and A.W. Decho, *A laboratory investigation of cyanobacterial extracellular polymeric secretions (EPS) in influencing CaCO3 polymorphism.* Journal of Crystal Growth, 2002. **240**(1-2): pp. 230-235.

45. Roberts, J.A., et al., *Microbial precipitation of dolomite in methanogenic groundwater.* Geology, 2004. **32**(4): pp. 277-280.

46. Van Lith, Y., et al., *Microbial fossilization in carbonate sediments: a result of the bacterial surface involvement in dolomite precipitation.* Sedimentology, 2003. **50**(2): pp. 237-245.

47. SchultzeLam, S., et al., *Mineralization of bacterial surfaces.* Chemical Geology, 1996. **132**(1-4): pp. 171-181.

48. Rodriguez-Navarro, C., et al., *Conservation of ornamental stone by Myxococcus xanthus-induced carbonate biomineralization.* Applied and Environmental Microbiology, 2003. **69**(4): pp. 2182-2193.

49. Arp, G., J. Hofmann, and J. Reitner, *Microbial fabric formation in spring mounds ("Microbialites") of alkaline salt lakes in the Badain Jaran Sand Sea, PR China.* Palaios, 1998. **13**(6): pp. 581-592.

50. Chafetz, H.S., P.F. Rush, and N.M. Utech, *Microenvironmental controls on mineralogy and habit of CaCO$_3$ precipitates - an example from an active travertine system.* Sedimentology, 1991. **38**(1): pp. 107-126.

51. Folk, R.L., H.S. Chafetz, and P.A. Tiezzi, *Bizarre forms of depositional and diagenetic calcite in hot-spring travertines, central Italy*, in *Carbonate cements*, N. Schneidermann and P.M. Harris, Editors. 1985, SEPM, Special Publication: Tulsa, Oklahoma, U.S.A. pp. 349-369.

52. Arp, G., A. Reimer, and J. Reitner, *Photosynthesis-induced biofilm calcification and calcium concentrations in phanerozoic oceans.* Science, 2001. **292**(5522): pp. 1701-1704.

53. Grotzinger, J.P. and N.P. James, *Precambrian carbonates: evolution of understanding*, in *Carbonate sedimentation and diagenesis in the evolving Precambrian world*, J.P.J. Grotzinger, Noel P, Editor. 2000, SEPM, Special Publication: Tulsa, OK. pp. 3-20.

54. Beech, I.B., et al., *Extracellular polysaccharides from Desulfovibrio desulfuricans and Pseudomonas fluorescens in the presence of mild and stainless steel.* Applied Microbiology and Biotechnology, 1991. **35**: pp. 65-71.

55. Feio, M.J., et al., *Isolation and characterisation of a novel sulphate-reducing bacterium of the Desulfovibrio genus.* Anaerobe, 1998. **4**(2): pp. 117-130.

56. Gerhardt, P., editor-in-chief ; R.G.E. Murray, Willis A. Wood, Noel R. Krieg, eds., *Methods for General and Molecular Bacteriology.* 1994, Washington, D.C.: American Society for Microbiology. 791.

57. Bradford, M.M., *Rapid and sensitive method for quantitation of microgram quantities of protein utilizing principle of protein-dye binding.* Analytical Biochemistry, 1976. **72**(1-2): pp. 248-254.

58. Blumenkrantz, N. and G. Asboehansen, *New method for quantitative-determination of uronic acids.* Analytical Biochemistry, 1973. **54**(2): pp. 484-489.

59. Allison, D.G. and I.W. Sutherland, *A staining technique for attached bacteria and its correlation to extracellular carbohydrate production.* Journal of Microbiological Methods, 1984. **2**(2): pp. 93-99.

60. Klug, H.P. and L.E. Alexander, *X-ray diffraction procedures for polycrystalline and amorphous materials.* 1954, New York: Wiley. 716.

61. Teng, H.H., et al., *Thermodynamics of calcite growth: Baseline for understanding biomineral formation.* Science, 1998. **282**(5389): pp. 724-727.

62. Tiller, W.A., *The science of crystallization: macroscopic phenomena and defect generation.* 1991, Cambridge, U.K.: Cambridge University Press. 484.

63. Meldrum, F.C. and S.T. Hyde, *Morphological influence of magnesium and organic additives on the precipitation of calcite.* Journal of Crystal Growth, 2001. **231**(4): pp. 544-558.

64. Astilleros, J.M., et al., *Molecular-scale surface processes during the growth of calcite in the presence of manganese.* Geochimica et Cosmochimica Acta, 2002. **66**(18): pp. 3177-3189.

65. Takasaki, S., K.I. Parsiegla, and J.L. Katz, *Calcite growth and the inhibiting effect of iron(III).* Journal of Crystal Growth, 1994. **143**(3-4): pp. 261-268.

66. Ferris, F.G., *Metallic ion interactions with the outer membrane of Gram-negative bacteria*, in *Metal ions and bacteria*, T.J. Beveridge and R.J. Doyle, Editors. 1989, John Wiley & Sons, Inc.: New York. pp. 295-323.

67. Mann, S., et al., *Morphological influence of functionalized and non-functionalized alpha,omega-dicarboxylates on calcite crystallization.* Journal of the Chemical Society, Faraday Transactions, 1990. **86**(10): pp. 1873-1880.

68. Jimenez-Lopez, C., et al., *Influence of lysozyme on the precipitation of calcium carbonate: A kinetic and morphologic study.* Geochimica et Cosmochimica Acta, 2003. **67**(9): pp. 1667-1676.

69. Adams, A.E. and W.S. MacKenzie, *A color atlas of carbonate sediments and rocks under the microscope*. 1998, New York: John Wiley & Sons. 180.

70. Reitner, J. and F. Neuweiler, *Mud mounds: A polygenetic spectrum of fine-grained carbonate buildups.* Facies, 1995. **32**: pp. 1-70.

71. Reid, R.P., *Nonskeletal peloidal precipitates in Upper Triassic reefs, Yukon Territory (Canada).* Journal of Sedimentary Petrology, 1987. **57**(5): pp. 893-900.

72. Sun, S.Q. and V.P. Wright, *Peloidal fabrics in Upper Jurassic reefal limestones, Weald Basin, southern England.* Sedimentary Geology, 1989. **65**: pp. 165-181.

73. Guo, L. and R. Riding, *Microbial micritic carbonates in uppermost Permian reefs, Sichuan Basin, southern China: some similarities with Recent travertines.* Sedimentology, 1992. **39**: pp. 37-53.

74. Adachi, N., Y. Ezaki, and J. Liu, *The fabrics and origins of peloids immediately after the end-Permian extinction, Guizhou Province, South China.* Sedimentary Geology, 2004. **164**: pp. 161-178.

75. Garcia-Mondejar, J. and P.A. Fernandez-Mendiola, *Albian carbonate mounds: comparative study in the context of sea-level variations (Soba, northern Spain)*, in

Carbonate Mud-Mounds: Their Origin and Evolution, C.L.V. Monty, et al., Editors. 1995, Blackwell Science: Oxford. pp. 359-384.

76. Pope, M.C., J.P. Grotzinger, and B.C. Schreiber, *Evaporitic subtidal stromatolites produced by in situ precipitation: textures, facies associations, and temporal significance.* Journal of Sedimentary Petrology, 2000. **70**: pp. 1139-1151.

77. Knoll, A.H. and M.A. Semikhatov, *The genesis and time distribution of two distinctive Proterozoic stromatolite microstructures.* Palaios, 1998. **13**: pp. 408-422.

78. Lighty, R.G., *Preservation of internal reef porosity and diagenetic sealing of submerged Early Holocene barrier reef, southeast Florida shelf*, in *Carbonate cements*, N. Schneidermann and P.M. Harris, Editors. 1985, SEPM: Tulsa, OK, USA. pp. 123-151.

79. Macintyre, I.G., *Submarine cements - The peloidal question*, in *Carbonate cements*, N. Schneidermann and P.M. Harris, Editors. 1985, SEPM: Tulsa, OK. pp. 109-116.

80. Jones, B., *Calcite Rafts, Peloids, and micrite in cave deposits from Cayman Brac, British-West-Indies.* Canadian Journal of Earth Sciences, 1989. **26**(4): pp. 654-664.

81. Folk, R.L. and H.S. Chafetz, *Bacterially induced microscale and nanoscale carbonate precipitates*, in *Microbial Sediments*, R.E. Riding and S.M. Awramik, Editors. 2000, Springer-Verlag: Berlin Heidelberg. pp. 41-49.

82. James, N.P., D.S. Marszalek, and P.W. Choquette, *Facies and fabric specificity of early subsea cements in shallow Belize (British Honduras) reefs.* Journal of Sedimentary Petrology, 1976. **46**: pp. 523-544.

83. Alexandersson, E.T., *Intragranular growth of marine aragonite and Mg-calcite: Evidence of precipitation from supersaturated seawater.* Journal of Sedimentary Petrology, 1972. **42**: pp. 441-460.

84. Macintyre, I.G., *Distribution of submarine cements in a modern Carribean fringing reef, Galeta Point, Panama.* Journal of Sedimentary Petrology, 1977. **47**: pp. 503-516.

85. Tribovillard, N.P., *Cyanobacterially generated peloids in laminated, organic-matter rich, limestones: an unobtrusive presence.* Terra Nova, 1998. **10**(3): pp. 126-130.

86. Reitner, J., *Modern cryptic microbialite/metazoan facies from Lizard Island (Great Barrier Reef, Australia): formation and concepts.* Facies, 1993. **29**: pp. 3-40.

87. Chafetz, H.S., *Marine Peloids - a Product of Bacterially Induced Precipitation of Calcite.* Journal of Sedimentary Petrology, 1986. **56**(6): pp. 812-817.

88. Chafetz, H.S. and R.L. Folk, *Travertines: Depositional morphology and the bacterially constructed constituents.* Journal of Sedimentary Petrology, 1984. **54**: pp. 289-316.

89. Kazmierczak, J., et al., *Cyanobacterial key to the genesis of micritic and peloidal limestones in ancient seas.* Acta Palaeontologica Polonica, 1996. **41**: pp. 319-338.

90. Glauert, A.M., *Fixation, dehydration and embedding of biological samples*, in *Practical methods in electron microscopy*, A.M. Glauert, Editor. 1975, Elsevier North-Holland Biomedical Press: Amsterdam. pp. 48.

91. Wierzchos, J. and C. Ascaso, *Application of back-scattered electron imaging to the study of the lichen-rock interface.* Journal of Microscopy, 1994. **175**: pp. 54-59.

92. Farmer, V.C.E., *The infrared spectra of minerals*. Vol. 4. 1974, London: Mineralogical Society. 539.

93. Aissaoui, D.M., *Magnesian calcite cements and their diagenesis: dissolution and dolomitization, Mururoa Atoll.* Sedimentology, 1988. **35**: pp. 821-841.

94. González, L.A., S.J. Carpenter, and K.C. Lohmann, *Inorganic calcite morphology - Roles of fluid chemistry and fluid-flow.* Journal of Sedimentary Petrology, 1992. **62**(3): pp. 382-399.

95. Taylor, J.C.M. and L.V. Illing, *Holocene intertidal calcium carbonate cementation, Qatar, Persian Gulf.* Sedimentology, 1969. **12**: pp. 618-634.

96. Council, T.C. and P.C. Bennett, *Geochemistry of ikaite formation at Mono Lake, California: Implications for the origin of tufa mounds.* Geology, 1993. **21**: pp. 971-974.

97. Riding, R., *Temporal variation in calcification in marine cyanobacteria.* Journal of the Geological Society, London, 1992. **149**: pp. 979-989.

98. Grotzinger, J.P. and A.H. Knoll, *Anomalous carbonate precipitates: Is the precambrian the key to the Permian?* Palaios, 1995. **10**(6): pp. 578-596.

99. Riding, R. and L. Liang. *Marine limestone accumulation over the past 550 million years: control by seawater chemistry*. in *Goldschmidt Conference*. 2004. Copenhagen: Geochimica and Cosmochimica Acta.

100. Raz, S., et al., *The transient phase of amorphous calcium carbonate in sea urchin larval spicules: The involvement of proteins and magnesium ions in its formation and stabilization.* Advanced Functional Materials, 2003. **13**(6): p. 480-486.

101. Vogel, K., et al., *Experimental studies on microbial bioerosion at Lee Stocking Island, Bahamas and One Tree Island, Great Barrier Reef, Australia: implications for paleoecological reconstructions.* Lethaia, 2000. **33**(3): pp. 190-204.

102. Brasier, M.D., et al., *Questioning the evidence for Earth's oldest fossils.* Nature, 2002. **416**(6876): pp. 76-81.

103. Schopf, J.W., et al., *Laser-Raman imagery of Earth's earliest fossils.* Nature, 2002. **416**(6876): pp. 73-76.

104. Vali, H., et al., *Nanoforms: A new type of protein-associated mineralization.* Geochimica Et Cosmochimica Acta, 2001. **65**(1): pp. 63-74.

105. Chafetz, H.S. and S.A. Guidry, *Bacterial shrubs, crystal shrubs, and ray-crystal shrubs: bacterial vs. abiotic precipitation.* Sedimentary Geology, 1999. **126**: pp. 57-74.

106. Wilkinson, B.H., A.L. Smith, and K.C. Lohmann, *Sparry Calcite Marine Cement in Upper Jurassic Limestones of Southeastern Wyoming*, in *Carbonate cements*, N. Schneidermann and P.M. Harris, Editors. 1985, The Society of Economic Paleontologists and Mineralogists: Tulsa. pp. 169-184.

107. Webb, G.E., J.S. Jell, and J.C. Baker, *Cryptic intertidal microbialites in beachrock, Heron Island, Great Barrier Reef: implications for the origin of microcrystalline beachrock cement.* Sedimentary Geology, 1999. **126**(1-4): pp. 317-334.

108. Chafetz, H.S. and J.C. Meredith, *Recent travertine pisoliths (pisoids) from southeastern Idaho, U.S.A.*, in *Coated Grains*, T.M. Peryt, Editor. 1983, Springer: New York.

109. Guo, L. and R. Riding, *Origin and diagenesis of Quaternary travertine shrub fabrics, Rapolano Terme, Italy.* Sedimentology, 1994. **41**: pp. 499-520.

110. Fraser, M.L. and F.A. Corsetti, *Neoproterozoic carbonate shrubs: Interplay of microbial activity and unusual environmental conditions in Post-Snowball Earth oceans.* Palaios, 2003. **18**: pp. 378-387.

111. Souza-Egipsy, V., et al. *Abiogenic layered carbonates associated with serpentinization: Why Martian "Stromatolites" might not be fossils*. in *Third European Workshop on Exo-Astrobiology. Mars: The search for life*. 2003. Madrid, Spain.

112. Madigan, M.T., J.M. Martinko, and J. Parker, *Brock biology of microorganisms*. 2000, New Jersey: Prentice Hall. 990.

113. Roedder, E., *Fluid inclusions*. Reviews in Mineralogy, ed. P.H. Ribbe. Vol. 12. 1984, Blacksburg, VA: Mineralogical society of America. 644.

114. Moore, C.H., *Carbonate diagenesis and porosity*. Developments in Sedimentology. Vol. 46. 1989, Amsterdam, The Netherlands: Elsevier Science Publishers B. V. 338.

115. Laval, B., et al., *Modern freshwater microbialite analogues for ancient dendritic reef structures*. Nature, 2000. **407**(6804): pp. 626-629.

116. Thompson, J.A. and S. Douglas. *Microbial mat from a hypersaline pond, Lee Stocking Island, Bahamas*. in *Geological Society of America*. 2002. Denver, CO: GSA.

117. Althukair, A.A. and S. Golubic, *New Endolithic cyanobacteria from the Arabian Gulf .1. Hyella- Immanis Sp-Nov*. Journal of Phycology, 1991. **27**(6): pp. 766-780.

118. Callot, G., et al., *Biogenic etching of microfractures in amorphous and crystalline silicates*. Nature, 1987. **328**(9): pp. 147-149.

119. Fouke, B.W., et al., *Depositional facies and aqueous-solid geochemistry of travertine-depositing hot springs (Angel Terrace, Mammoth Hot Springs, Yellowstone National Park, USA)*. Journal of Sedimentary Research, 2000. **70**(3): pp. 565-585.

120. Krumbein, W.E., Y. Cohen, and M. Shilo, *Solar Lake (Sinai) IV. Stromatolitic cyanobacterial mats*. Limnology and Oceanography, 1977. **22**: pp. 635-656.

121. Desmarais, D.J. and H. Bui, *Carbon isotopic studies of microbial mats and stromatolites*. Origins of Life and Evolution of the Biosphere, 1986. **16**(3-4): pp. 343-343.

122. Kawaguchi, T. and A.W. Decho, *Isolation and biochemical characterization of extracellular polymeric secretions (EPS) from modern soft marine stromatolites (Bahamas) and its inhibitory effect on CaCO3 precipitation*. Preparative Biochemistry & Biotechnology, 2002. **32**(1): pp. 51-63.

123. Walter, M.R., J. Bauld, and T.D. Brock, *Microbiology and morphogenesis of columnar stromatolites (Conophyton, Vacerilla) from hot springs in Yellowstone National Park*, in *Stromatolites*, M.R. Walter, Editor. 1976, Elsevier Scientific Publishing Company: New York. pp. 790.

124. Abed, R.M.M., et al., *Characterization of microbialite-forming cyanobacteria in a tropical lagoon: Tikehau Atoll, Tuamotu, French Polynesia*. J. Phycol., 2003. **39**: pp. 862-873.

125. Turing, A., *The chemical basis of morphogenesis*. Phil Trans B, 1952. **237**: pp. 37-72.

126. Budrene, E.O. and H.C. Berg, *Dynamics of formation of symmetrical patterns by chemotactic bacteria*. Nature, 1995. **376**(6535): pp. 49-53.

127. Budrene, E.O. and H.C. Berg, *Complex patterns formed by motile cells of Escherichia-coli.* Nature, 1991. **349**(6310): pp. 630-633.

128. Mittal, N., et al., *Motility of Escherichia coli cells in clusters formed by chemotactic aggregation.* Proceedings of the National Academy of Sciences of the United States of America, 2003. **100**(23): pp. 13259-13263.

129. Huang, X., Y.Q. Dong, and J.D. Zhao, *HetR homodimer is a DNA-binding protein required for heterocyst differentiation, and the DNA-binding activity is inhibited by PatS.* Proceedings of the National Academy of Sciences of the United States of America, 2004. **101**(14): pp. 4848-4853.

130. Li, J.H., et al., *An increase in the level of 2-oxoglutarate promotes heterocyst development in the cyanobacterium Anabaena sp strain PCC 7120.* Microbiology-Sgm, 2003. **149**: pp. 3257-3263.

131. Gruber, T.M. and C.A. Gross, *Multiple sigma subunits and the partitioning of bacterial transcription space.* Annual Review of Microbiology, 2003. **57**: pp. 441-466.

132. Figge, R.M. and J.W. Gober, *Cell shape, division and development: the 2002 American Society for Microbiology (ASM) conference on prokaryotic development.* Molecular Microbiology, 2003. **47**(5): pp. 1475-1483.

133. Stanley, N.R. and B.A. Lazazzera, *Environmental signals and regulatory pathways that influence biofilm formation.* Molecular Microbiology, 2004. **52**(4): pp. 917-924.

134. Moorthy, S. and P.I. Watnick, *Genetic evidence that the Vibrio cholerae monolayer is a distinct stage in biofilm development.* Molecular Microbiology, 2004. **52**(2): pp. 573-587.

135. Ramsey, M.M. and M. Whiteley, *Pseudomonas aeruginosa attachment and biofilm development in dynamic environments.* Molecular Microbiology, 2004. **53**(4): pp. 1075-1087.

136. Bhaya, D., A. Takahashi, and A.R. Grossman, *Light regulation of type IV pilus-dependent motility by chemosensor-like elements in Synechocystis PCC6803.* Proceedings of the National Academy of Sciences of the United States of America, 2001. **98**(13): pp. 7540-7545.

137. Mattick, J.S., *Type IV pili and twitching motility.* Annual Review of Microbiology, 2002. **56**: pp. 289-314.

138. Armitage, J.P. and K.J. Hellingwerf, *Light-induced behavioral responses ('phototaxis') in prokaryotes.* Photosynthesis Research, 2003. **76**(1-3): pp. 145-155.

139. Zhang, L.H. and Y.H. Dong, *Quorum sensing and signal interference: diverse implications.* Molecular Microbiology, 2004. **53**(6): pp. 1563-1571.

140. Hammer, B.K. and B.L. Bassler, *Quorum sensing controls biofilm formation in Vibrio cholerae (vol 50, pg 101, 2003).* Molecular Microbiology, 2004. **51**(5): pp. 1521-1521.

141. Brehm, U., W.E. Krumbein, and K.A. Palinska, *Microbial spheres: a novel cyanobacterial-diatom symbiosis.* Naturwissenschaften, 2003. **90**: pp. 136-140.

142. Kawata, T., et al., *SH2 signaling in a lower eukaryote: A STAT protein that regulates stalk cell differentiation in Dyctyostelium.* Cell, 1997. **89**: pp. 909-916.

143. Olson, J.M. and R.E. Blankenship, *Thinking about the evolution of photosynthesis.* Photosynthesis Research, 2004. **80**(1-3): p. 373-386.

144. Tobin, K.J., *The paleoecology and significance of the Gunflint-type microbial assemblages from the Frere Formation (Early Proterozoic), Nabberu Basin, Western-Australia.* Precambrian Research, 1990. **47**(1-2): pp. 71-81.

145. Thompson, J.B., et al., *Whiting events: Biogenic origin due to the photosynthetic activity of cyanobacterial picoplankton.* Limnology and Oceanography, 1997. **42**(1): pp. 133-141.

146. Pinckney, J.L. and H.W. Paerl, *Anoxygenic photosynthesis and nitrogen fixation by a microbial mat community in a Bahamian hypersaline lagoon.* Applied and Environmental Microbiology, 1997. **63**(2): pp. 420-426.

147. Wang, X., H.V. Modak, and F.R. Tabita, *Photolithoautotrophic growth and control of Co2 fixation in Rhodobacter-sphaeroides and Rhodospirillum-rubrum in the absence of ribulose-bisphosphate carboxylase-oxygenase.* Journal of Bacteriology, 1993. **175**(21): pp. 7109-7114.

148. Rothschild, L.J. and R.L. Mancinelli, *Model of carbon fixation in microbial mats from 3,500 Myr ago to the Present.* Nature, 1990. **345**(6277): pp. 710-712.

149. Morel, F.M.M. and J.G. Hering, *Principles and applications of aquatic chemistry.* 1993, New York: John Wiley & Sons, Inc. 588.

150. Monty, C.L.V., *The origin and development of cryptalgal fabrics*, in *Stromatolites*, M.R. Walter, Editor. 1976, Elsevier Scientific Publishing Company: Amsterdam, The Netherlands. pp. 193-250.